Piecewise Tendency Diagnosis of Dynamical Processes Governing the Development of an Upper-Tropospheric Mobile Trough

JOHN W. NIELSEN-GAMMON AND RANDY J. LEFEVRE*

Department of Meteorology, Texas A&M University, College Station, Texas

(Manuscript received 17 January 1996, in final form 2 May 1996)

ABSTRACT

The intensification and evolution of midlatitude upper-tropospheric mobile troughs may be viewed in terms of the isentropic advection and deformation of the tropopause potential vorticity gradient. The potential vorticity viewpoint allows one to qualitatively assess observed events in the context of existing theories of mobile trough genesis, such as baroclinic instability or downstream development. In order to quantitatively determine the role of distinct dynamical processes, the method of piecewise tendency diagnosis, or PTD, is developed. PTD is an extension of piecewise potential vorticity inversion applied to height tendencies, with the forcing terms in the quasigeostrophic height tendency equation partitioned into potential vorticity advection associated with distinct dynamical processes.

A particular case of mobile trough genesis, which occurred during 1–4 December 1980 over North America, is diagnosed using PTD. Although about 20% of the intensification of the trough was due to superposition and amplification of the low-level cyclone during surface cyclogenesis, the diagnosis focuses on the height perturbation induced by the upper-level PV anomaly. The trough is found to have formed primarily through downstream propagation of Rossby wave energy from disturbances over the northwest Pacific. As the trough amplified, it interacted with an existing surface temperature gradient over the central United States and produced a frontal wave. As the frontal wave intensified, the favorable vertical tilt allowed mutual baroclinic amplification of the upper and lower systems. Eventually, the upper-level trough grew to sufficient amplitude that it began to lose energy downstream through wave propagation and the trough began to weaken even though a favorable tilt remained between the upper and lower systems. Horizontal deformation and small-scale vortex interaction were less important to the overall development of the mobile trough, but contributed significantly to intensification at various times in its life cycle. The direct effects of the remaining dynamical processes (excluding latent heating and friction, which were not diagnosed) were insignificant.

1. Introduction

Mobile troughs in the middle and upper troposphere are the triggers for most extratropical cyclogenesis events. While the simultaneous growth of disturbances in the upper and lower troposphere has been studied extensively, primarily in the context of baroclinic instability theory, comparatively little attention has been paid to the origin of the incipient mobile trough prior to the onset of troposphere-deep cyclogenesis. The purposes of this study are to develop a quantitative diagnostic technique, which is based upon potential vorticity (PV) and is capable of distinguishing between dynamical mechanisms for development, and to apply this technique to a case of mobile trough formation and intensification over the United States.

Recent interest in upper-tropospheric mobile troughs has been stimulated by a study by Sanders (1988). Sanders constructed a climatology of troughs found along the 552-dam geopotential height contour of the 500-mb surface by subjectively identifying and tracking troughs on daily Northern Hemisphere analyses. Sanders found, and a subsequent objective climatology by Lefevre and Nielsen-Gammon (1995) confirmed, that preferred regions of mobile trough genesis lie over continents, upstream of the preferred regions of surface cyclone genesis over the western oceans (e.g., Petterssen 1956). Lefevre and Nielsen-Gammon also demonstrated that the lifetimes of 500-mb mobile troughs exhibit a Poisson distribution, with a median lifetime of about 5 days. The observed long duration of mobile troughs has been reproduced in a model with concentrated PV gradients at the tropopause (Rivest et al. 1992).

* Current affiliation: Air Force Global Weather Central, Offutt Air Force Base, Omaha, Nebraska

Corresponding author address: John W. Nielsen-Gammon, MS 3150, Dept. of Meteorology, Texas A&M University, College Station, TX 77843-3150.
E-mail: n-g@tamu.edu

Nielsen-Gammon (1995) identified and discussed four basic mechanisms that have been postulated to produce intensification of upper-level mobile troughs: modal instability (e.g., Whitaker and Barcilon 1992; Snyder and Lindzen 1988), nonmodal growth (e.g., Rivest and Farrell 1992), propagation of wave energy (e.g., Simmons and Hoskins 1979), and superposition (e.g., Farrell 1989b). A composite case study by Sanders (1988) suggested that baroclinic instability may serve as a generating mechanism, while two case studies (Orlanski and Sheldon 1993; Nielsen-Gammon 1995) have implicated propagation of wave energy and subsequent baroclinic intensification, a process which Orlanski and Sheldon call downstream baroclinic development.

In their studies of downstream baroclinic development, Orlanski and coworkers (Orlanski and Katzfey 1991; Chang 1993; Orlanski and Chang 1993; Orlanski and Sheldon 1993; Chang and Orlanski 1994; Orlanski and Sheldon 1995) have relied on energetics as a diagnostic tool. While energetics analyses have provided valuable insight into a wide variety of problems in atmospheric dynamics, two shortcomings in particular hinder their applicability to individual observed cyclogenesis events. First, energetics may be incapable of distinguishing between certain important but inherently dissimilar dynamical processes. For example, the energetics of a Charney (1947) normal mode may be quite similar to the waves discussed by Farrell (1985), which extract energy from the vertical shear and grow rapidly despite being stable to baroclinic instability. Second, quantitative study of the energetics of a cyclone requires specification of a volume of integration and boundaries through which energy may travel, making it difficult to attribute growth to specific elements of the evolving system.

The objective of this paper is to develop a complementary diagnostic technique, essentially a quantitative version of "potential vorticity thinking" (Hoskins et al. 1985), and to apply it to an observed case of upper-tropospheric mobile trough generation and intensification. This technique, called piecewise tendency diagnosis (PTD), is an extension of piecewise potential vorticity inversion (Davis and Emanuel 1991; Davis 1992a), except that the potential vorticity *advection* is partitioned and elements of the overall height tendency due to particular dynamical processes are isolated.

In section 2, we present the quasigeostrophic potential vorticity form of the height tendency equation (the QGPV height tendency equation). The following section describes the application of the QGPV height tendency equation to several simple dynamical phenomena, illustrating the PTD technique and identifying several subtleties involved in the application of the equation. The case study, dataset, and implementation of PTD are described in section 4. The results for the evolution of the mobile trough are presented in section 5. Section 6 contains a concluding discussion.

2. The QGPV height tendency equation

The quasigeostrophic potential vorticity q, or pseudopotential vorticity, may be defined as

$$q = f + \frac{1}{f_0}\nabla^2\varphi + f_0\frac{\partial}{\partial p}\left(\frac{1}{\sigma}\frac{\partial\varphi}{\partial p}\right) = f + \pounds(\varphi) \quad (2.1)$$

(Charney and Stern 1962), using pressure as a vertical coordinate, and with f, f_0, and σ defined as in Holton (1993, chapter 6). The Laplacian-like operator £ may be inverted, using suitable boundary conditions (Hoskins et al. 1985), to obtain the geopotential φ distribution from the q distribution:

$$\varphi = \pounds^{-1}(q - f). \quad (2.2)$$

The lower boundary condition (at $p = p_b$) is conventionally specified using the boundary potential temperature θ:

$$\frac{\partial\varphi}{\partial p} = -\frac{R}{p}\left(\frac{p}{p_0}\right)^{R/c_p}\theta. \quad (2.3)$$

Because the operator £ is linear, a height tendency equation, with boundary conditions, may be obtained by taking the local time derivative of (2.1) (e.g., Holton 1993) and inverting, together with the time derivative of (2.3):

$$\frac{\partial q}{\partial t} = \frac{1}{f_0}\nabla^2\left(\frac{\partial\varphi}{\partial t}\right) + f_0\frac{\partial}{\partial p}\left(\frac{1}{\sigma}\frac{\partial}{\partial p}\left(\frac{\partial\varphi}{\partial t}\right)\right) = \pounds\left(\frac{\partial\varphi}{\partial t}\right) \quad (2.4)$$

$$\frac{\partial\varphi}{\partial t} = \pounds^{-1}\left(\frac{\partial q}{\partial t}\right) \quad (2.5)$$

$$\frac{\partial}{\partial p}\left(\frac{\partial\varphi}{\partial t}\right) = -\frac{R}{p}\left(\frac{p}{p_0}\right)^{R/c_p}\frac{\partial\theta}{\partial t}. \quad (2.6)$$

According to the quasigeostrophic system, the local rate of change of q is given by the geostrophic advection of q, diabatic generation and destruction, and frictional generation and destruction. Similarly, the local rate of change of θ is given by the geostrophic advection of θ, diabatic generation and destruction, and vertical advection. Near the ground, where (2.6) will be applied, the vertical advection term reduces to topographic forcing: cooling and heating by upslope and downslope flow.

In this study diabatic, frictional, topographic, and nonquasigeostrophic processes will be neglected in the computation of φ tendencies. However, any q or θ variations produced by these processes and present in the analyses will affect φ in a manner equivalent to adiabatically generated q or θ variations. For example, consider a lower-tropospheric anomaly produced by latent heating. Its instantaneous effect on the intensity of an

upper-level trough depends on the advection of upper-level potential vorticity by the winds it induces and is independent of the process responsible for the generation of the lower-tropospheric anomaly itself. Similar arguments apply to frictional and topographic processes, which are commonly modeled in the quasigeostrophic system as affecting surface θ but do not directly affect upper-level potential vorticity. Since this study will focus on changes taking place in the upper tropospheric trough, direct diabatic and frictional effects are likely to be small.

Assuming that the flow is adiabatic and frictionless and the lower boundary is flat, (2.5) and (2.6) may be rewritten in the form used in this study:

$$g\frac{\partial Z}{\partial t} = \frac{\partial \varphi}{\partial t} = \pounds^{-1}(-\mathbf{v}\cdot\nabla q) \tag{2.7}$$

$$g\frac{\partial}{\partial p}\left(\frac{\partial Z}{\partial t}\right) = \frac{\partial}{\partial p}\left(\frac{\partial \varphi}{\partial t}\right) = -\frac{R}{p}\left(\frac{p}{p_0}\right)^{R/c_p}(-\mathbf{v}\cdot\nabla\theta), \tag{2.8}$$

where $\mathbf{v}$ is the geostrophic wind vector and Z is the geopotential height. We refer to (2.7) as the QGPV height tendency equation. We shall also refer to height and geopotential interchangeably in the following discussion, since the two differ only by a constant. In this formulation, both θ and q are conserved following the geostrophic wind, and (in the Northern Hemisphere) regions of high values of surface θ, like regions of high values of interior q, are associated with positive vorticity and negative φ anomalies. Thus, the right-hand sides of both (2.7) and (2.8) may be regarded as "forcing" the φ tendencies.

Boundary conditions other than (2.8) are physically justifiable. Bishop and Thorpe (1994) advocate free-space Green's functions, such that the φ field associated with a particular anomaly is independent of its distance from a boundary. However, this technique introduces conceptual difficulties at the boundaries: the evolution of potential temperature anomalies, like the evolution of height anomalies, is no longer a local process. Hakim et al. (1996) tested several alternatives and settled on a technique in which the boundary variations directly beneath an anomaly are included in the boundary conditions. However, this technique is only suited to isolated anomalies and also makes interpretation of boundary θ evolution problematic. The use of (2.8) as a boundary condition preserves the analogy between boundary θ and interior q made explicit by Bretherton (1966) and is well suited to our objective of comparing the atmospheric evolution to baroclinic instability theory.

Bell and Bosart (1993) used the system (2.7) and (2.8) to investigate height tendencies during the development of an upper-tropospheric cutoff cyclone and performed piecewise inversions to determine the levels of potential vorticity advection important to the development of the cyclone. Davis et al. (1996) used analogous boundary conditions for solving a system of equations for height and streamfunction tendency based on nonlinear balance. Hakim et al. (1996) employed a system similar to (2.7–2.8), but with different boundary conditions as noted above, for inversion of potential vorticity tendencies.

3. Partitioning: Some simple examples

In this section, we describe the application of the QGPV tendency equation (2.7), with (2.8) applied on horizontal boundaries, to several dynamical systems. We wish to motivate piecewise tendency diagnosis by demonstrating the relationship between PV thinking and height tendencies, and by showing how specific elements of the height tendency forcing are attributable to particular dynamical processes, at least in simple systems.

a. Barotropic, one-dimensional Rossby wave

Consider a linear, monochromatic, barotropic Rossby wave embedded in a zonal westerly flow (Fig. 1). The motion of the wave is governed by two processes: the advection of the wave downstream by the environmental flow and the propagation of the wave upstream along the environmental q gradient.

The partitioning of the total flow into "wave" and "environment" is essential for describing the dynamics of even this simple system. The partitioning may be performed in several ways: time mean versus time varying, zonal mean versus zonally varying, and small zonal wavenumber (in this example, $k = 0$) versus large zonal wavenumber. Postponing discussion of this issue until later, we adopt the terms "large scale" or "basic state" for the environmental flow and "small scale" or "perturbation" for the wavelike flow, and designate large-scale and small-scale elements of the flow by overbars and primes, respectively:

$$q = \bar{q} + q' \tag{3.1a}$$

$$\mathbf{v} = \bar{\mathbf{v}} + \mathbf{v}' \tag{3.1b}$$

$$\varphi = \bar{\varphi} + \varphi'. \tag{3.1c}$$

Substituting into (2.7),

$$\underset{\text{A}}{\frac{\partial \bar{\varphi}}{\partial t}} + \underset{\text{B}}{\frac{\partial \varphi'}{\partial t}} = \underset{\text{C}}{\pounds^{-1}(-\bar{\mathbf{v}}\cdot\nabla\bar{q})} + \underset{\text{D}}{\pounds^{-1}(-\bar{\mathbf{v}}\cdot\nabla q')} + \underset{\text{E}}{\pounds^{-1}(-\mathbf{v}'\cdot\nabla\bar{q})} + \underset{\text{F}}{\pounds^{-1}(-\mathbf{v}'\cdot\nabla q')}. \tag{3.2}$$

Terms A, C, and F are identically zero because the large-scale fields are zonally uniform and the waves are linear. Term D represents the downstream advection of the wave by the large-scale flow, and term E governs the upstream propagation of the wave. We write

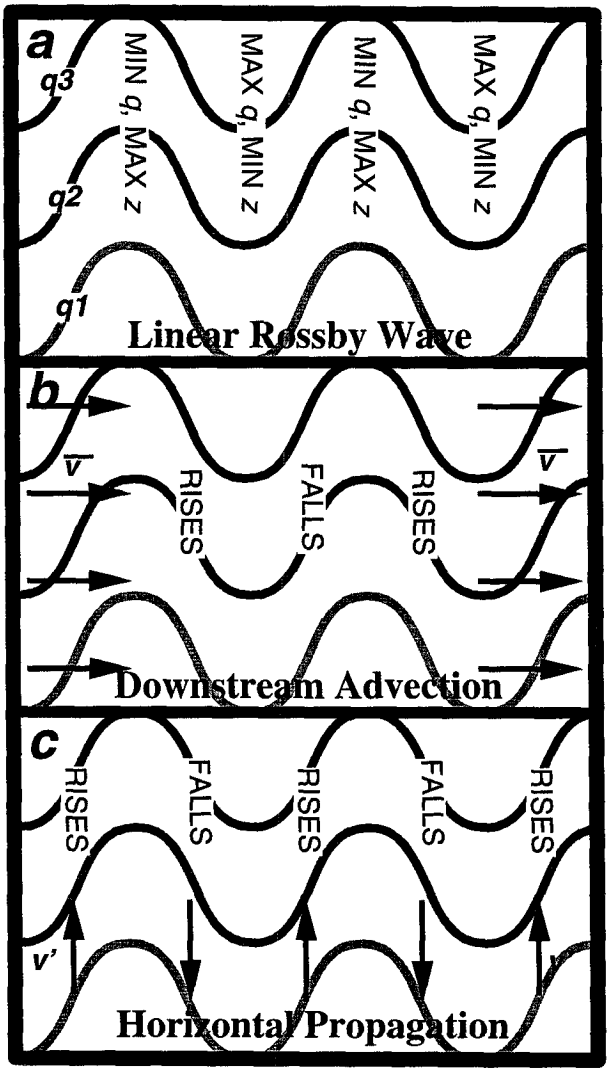

FIG. 1. (a) Schematic diagram of a linear, one-dimensional barotropic Rossby wave. Contours show QGPV distribution; $q1 < q2 < q3$. Also indicated are axes of extrema of perturbation QGPV and geopotential height. (b) Distribution of height rises and falls due to advection of QGPV by the basic-state wind. (c) Distribution of height rises and falls due to advection of basic-state QGPV by the perturbation wind.

$$\frac{\partial \varphi'}{\partial t} = \left(\frac{\partial \varphi'}{\partial t}\right)_{\text{ADV}} + \left(\frac{\partial \varphi'}{\partial t}\right)_{\text{PROP}} \tag{3.3a}$$

$$\left(\frac{\partial \varphi'}{\partial t}\right)_{\text{ADV}} = \pounds^{-1}(-\bar{\mathbf{v}}\cdot\nabla q') \tag{3.3b}$$

$$\left(\frac{\partial \varphi'}{\partial t}\right)_{\text{PROP}} = \pounds^{-1}(-\mathbf{v}'\cdot\nabla \bar{q}). \tag{3.3c}$$

As shown in Fig. 1, the advection by the large-scale wind induces height falls downstream of the troughs, while propagation, associated with meridional advection of the basic-state gradient, induces height falls upstream of the troughs. The net motion of the wave relative to the ground is determined by the relative magnitudes of the two tendencies.

If the intensity of a trough is defined as the *local minimum value of perturbation* (small scale) *height*, the *rate of intensification* is equal to the height *tendency* at the height *minimum*. In this example, neither advection nor propagation should affect the intensity of the troughs or ridges and, as seen in Fig. 1, the two height tendencies are each exactly 90° out of phase with the height anomalies.

b. Barotropic Rossby wave packet

Now consider the situation at the leading (eastern) edge of a Rossby wave packet (Fig. 2a). Individual ridges and troughs will increase in amplitude until the center of the wave packet passes them and will decrease thereafter. Some examples of this are discussed in Hoskins (1990).

Using the same definition as before, the rate of amplification of the cyclonic height perturbation is given by the height tendency at its center. The large-scale advection (3.3b) contributes nothing to this tendency; since the large-scale flow is uniform, it simply acts to translate the entire q' and φ' pattern downstream without change of amplitude. The intensification is due entirely to the propagation term (3.3c), and the magnitude of intensification is given by the value of this term at the location of the trough.

Viewed from the standpoint of PV advection, the southward flow must be partly in phase with the q' maximum, so that q' may locally amplify. This advection requires a phase shift between q' and φ'. The phase shift is related to the differing amplitudes of the adjoining negative q' anomalies (Fig. 2b). Consider the north–south wind at the location of the positive q' anomaly. The strong upstream negative q' anomaly will be associated with strong northerlies at that location, while the weaker downstream negative anomaly will be associated with weak southerlies. The net flow will thus be northerly, amplifying the positive anomaly.

The description is only slightly modified if one focuses on the φ' centers rather than the q' centers (Fig. 2c). Note that no advection of $\bar{q}$ exists at the center of the height anomalies, which is where the north–south flow is zero. A net height fall is felt at the center of the trough because the northerlies upstream of the trough are stronger than the southerlies downstream, so the positive advection of $\bar{q}$ to the west is felt more strongly [through (2.7)] than the negative advection to the east.

c. Barotropic deformation

In other situations, the large-scale advection produces intensification while the propagation term contributes nothing. For example, consider the basic state

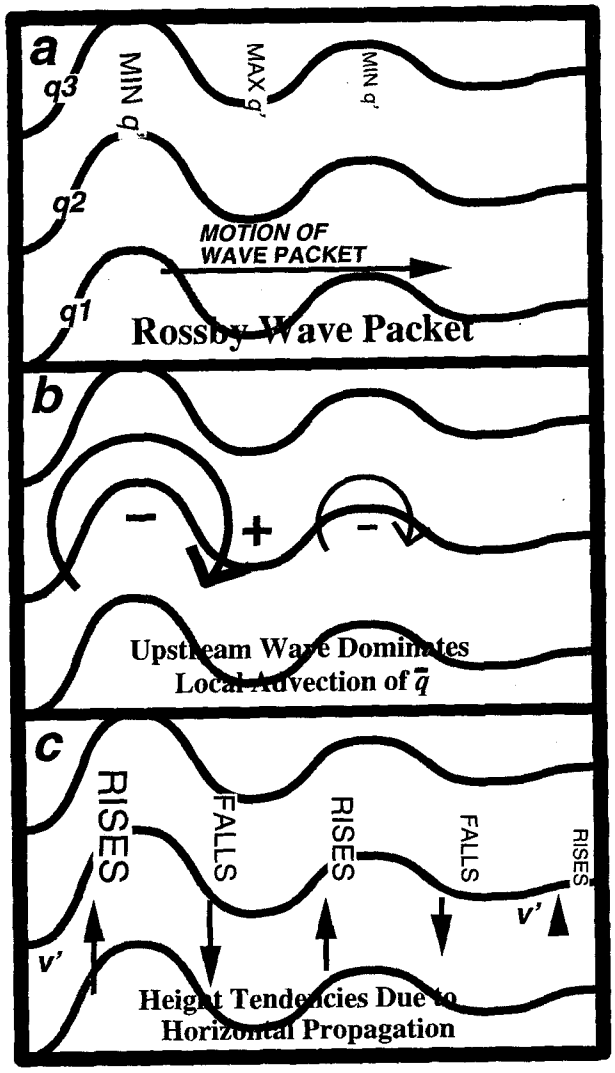

FIG. 2. (a) Schematic diagram of leading edge of a linear, barotropic Rossby wave packet. Contours and labels show QGPV distribution as in Fig. 1. (b) The northerly perturbation winds associated with the stronger upstream anomaly overwhelm the southerly perturbation winds associated with the weaker downstream anomaly, leading to net northerlies in phase with the positive QGPV anomaly and amplification of the anomaly. (c) Net pattern of north–south winds associated with the propagating wave and resulting height tendencies. Height tendencies are phase-shifted downstream from the advections, making them slightly in phase with the wave troughs and ridges and producing local amplification.

studied by Farrell (1989b): a large-scale confluent flow with no basic-state q gradient (Fig. 3), so that the propagation term is identically zero. A q' anomaly with its major axis oriented north–south, normal to the axis of dilatation, will be deformed by this flow into a more circular shape before becoming elongated in the direction of the axis of dilatation. While it becomes more circular, φ' increases in amplitude and the perturbation kinetic energy also increases.

Figure 3b shows that the redistribution of PV during intensification has the effect of moving two patches of high PV air toward the center of the anomaly from more distant locations. The height perturbation becomes more negative at the center of the anomaly as the patches move closer to the center. The most intense anomaly achievable through redistribution of potential vorticity would be circular. In three dimensions, with the vertical coordinate scaled by the ratio of the stratification and the Coriolis parameter, the most desirable distribution of potential vorticity is spherical.

The QGPV height tendency equation correctly diagnoses this process as being due to advection of the

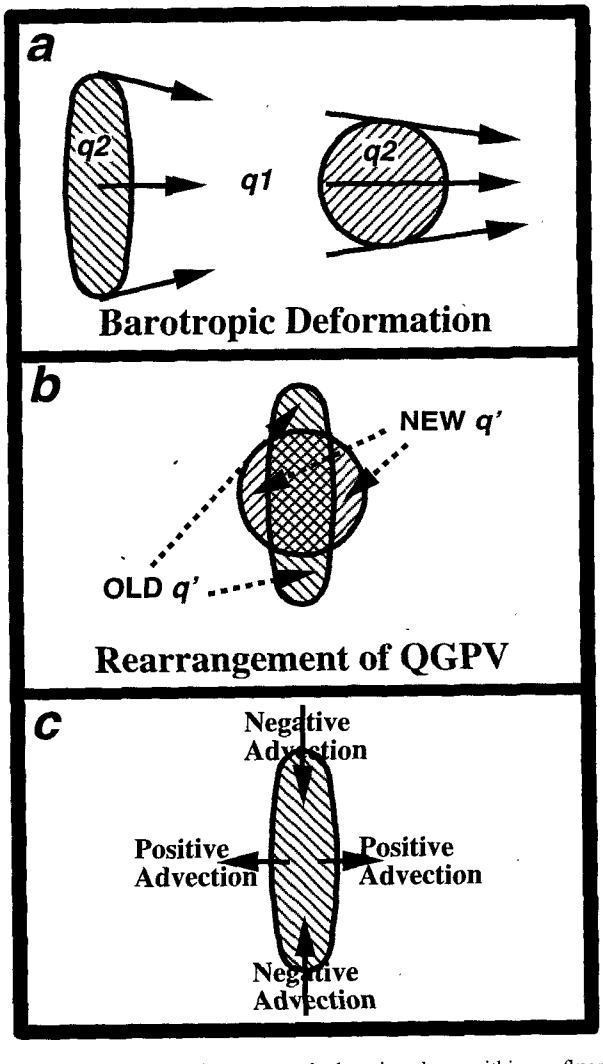

FIG. 3. (a) Idealized vortex patch changing shape within confluent flow. (b) Net redistribution of QGPV: potential vorticity is effectively moved from the extremities of the vortex patch to near the center of the vortex patch. The more compact the distribution of QGPV, the stronger the associated circulation. (c) QGPV advection pattern associated with the deformation flow, which produces net height falls near the center and net height rises to the north and south.

small-scale q field by the large-scale winds. In the q' advection field, the manner in which this occurs is best seen by choosing a frame of reference moving with the anomaly (Fig. 3c). The φ falls near the center are produced by positive q' advection along the east and west margins of the anomaly that, because of their proximity to the center, locally dominate the equally strong negative q' advection on the north and south ends of the anomaly.

For a discussion of a similar process involving two separate potential vorticity anomalies being brought into superposition by the background flow; see Hakim et al. (1996).

d. Eady normal mode cyclogenesis

The PV description of an Eady (1949) wave is given by Hoskins et al. (1985) and is briefly summarized here. The q' field [defined, following Bretherton (1966), as including the boundary θ' field] consists of two edge waves on the top and bottom boundaries. In isolation, the upper wave would tend to propagate to the west while being advected eastward, and the lower wave would tend to propagate to the east while being advected westward. With a favorable vertical tilt, the winds associated with the lower wave can advect θ on the upper boundary so as to amplify the upper wave, and the upper wave can do the same to the lower wave. In addition to allowing growth, the proper phase tilt also allows the waves to remain "in step," with fixed vertical tilt, because the winds associated with each wave can retard or accelerate the other.

To meet our objectives, the height tendency diagnosis must retain the conceptual framework and simplicity of this PV description. We proceed by distinguishing between the upper wave, the lower wave, and the gradients in which the two waves are embedded and neglect terms that are identically zero for the linear Eady problem. Consider the intensification of the height field associated with the upper-level wave alone, φ'_U, defined as

$$\varphi'_U = \pounds^{-1}(q'_U) \tag{3.5a}$$

$$\frac{\partial \varphi'_U}{\partial t} = \pounds^{-1}(-\mathbf{v}'_U \cdot \nabla \bar{q}_U) + \pounds^{-1}(-\mathbf{v}'_L \cdot \nabla \bar{q}_U) + \pounds^{-1}(-\bar{\mathbf{v}} \cdot \nabla q'_U). \tag{3.5b}$$

In our notation, the subscripted perturbation winds are the winds associated with the perturbation potential vorticity in the layer given by the subscript. For example, $\mathbf{v}'_L$ is the wind associated with the low-level perturbation potential vorticity (and surface potential temperature):

$$\mathbf{v}'_L = \frac{1}{f_0}\mathbf{k} \times \nabla(\pounds^{-1}(q'_L)), \tag{3.6}$$

which is inverted using the observed θ' as the lower boundary condition and $\theta' = 0$ as the upper boundary condition. The resulting velocity $\mathbf{v}'_L$ will generally be nonzero throughout the fluid. Also remember that, for the sake of brevity of discussion, q'_L includes the "effective" potential vorticity associated with the lower boundary θ'. The large-scale wind field $\bar{\mathbf{v}}$ is left unpartitioned, which avoids the large cancellations found by Holopainen and Kaurola (1991) that exist between winds induced by large-scale upper-level and lower-level effective PV gradients.

Of the three terms that involve alteration of the q' distribution at upper levels, only the advections of large-scale upper-level q associated with the low-level wave, the $\pounds^{-1}(-\mathbf{v}'_L \cdot \nabla \bar{q}_U)$ term, contributes to intensification and produces a nonzero φ'_U tendency at the location of a φ'_U extremum during pure normal mode cyclogenesis. The other two terms in (3.5b) affect the relative speed of the upper wave (as in section 3a) but do not directly contribute to intensification in the Eady model. In the analogous equation (not shown) for the evolution of heights associated with low-level potential vorticity, only the $\pounds^{-1}(-\mathbf{v}'_U \cdot \nabla \bar{q}_L)$ term produces intensification and leads to a nonzero tendency at the φ'_L minima. The amplification of the cyclone system is diagnosed as being due to anomalies on each PV gradient causing PV advection across the other gradient.

e. Midlatitude cyclogenesis: The general case

The critical step in the above analysis was considering separately the intensification of the height field associated with each anomaly or wave. The same method carries over to the more complex real atmosphere cases. The intensification of each PV anomaly must be diagnosed separately and the results combined to yield intensification of the overall system.

Typical cyclogenesis events involve one or more upper-tropospheric troughs that usually reside on the tropopause PV gradient, a surface θ wave embedded within a baroclinic zone, and (particularly at later stages) a vertical dipole of PV produced by latent heat release (Reed et al. 1992; Davis et al. 1993). The low-level positive PV anomaly produced by latent heat release is normally in phase with the surface warm anomaly, and latent heating in some theoretical models has been shown to play the same role as a surface θ gradient in the dynamics of baroclinic instability (Snyder and Lindzen 1991; Parker and Thorpe 1995). For simplicity, we shall therefore treat the surface θ and low-level PV collectively as a single entity analogous to the surface θ in the Eady model.

The upper-level intensification term is divided into six terms by starting with (3.2), allowing only advections of upper-level PV, and filtering the nonlinear terms to eliminate any large-scale tendencies. The terms are grouped according to their physical interpretation, as discussed below:

$$\frac{\partial \varphi'_U}{\partial t} = \mathcal{L}^{-1}(-\bar{\mathbf{v}}\cdot\nabla\bar{q}_U)' + \mathcal{L}^{-1}(-\bar{\mathbf{v}}\cdot\nabla q'_U)' + \mathcal{L}^{-1}(-\mathbf{v}'_U\cdot\nabla\bar{q}_U)' + \mathcal{L}^{-1}(-\mathbf{v}'_L\cdot\nabla\bar{q}_U)' + \mathcal{L}^{-1}(-\mathbf{v}'_U\cdot\nabla q'_U)' + \mathcal{L}^{-1}(-\mathbf{v}'_L\cdot\nabla q'_U)'. \quad (3.7)$$

Each term on the right-hand side is inverted independently, with $\partial/\partial p(\partial\varphi'_U/\partial t) = 0$ at the bottom and $\partial/\partial p(\partial\varphi'_U/\partial t)$ specified at the top by the advection of large-scale or small-scale θ by the large-scale or small-scale upper or lower winds, as appropriate.

The interpretation of each of the forcing terms is shown in Fig. 4. Many of these have been discussed above. The first term on the rhs of (3.7) represents nonlinear large-scale interaction, which in our case projects very little onto the small scale. The second term represents advection of small-scale PV by the large-scale flow and includes intensification processes such as barotropic deformation and horizontal superposition. The third term represents advection of large-scale PV by the small-scale wave and includes group velocity effects and downstream development. The fourth term, the baroclinic amplification term, is the advection of upper-level large-scale PV by winds associated with the low-level q' anomalies, including surface θ' anomalies. We use the term "baroclinic amplification" rather than "baroclinic instability" because fundamentally similar growth can occur through this basic advection process even when normal-mode baroclinic instability is not possible (e.g., Rotunno and Fantini 1989). Finally, the fifth and sixth terms represent small-scale interactions among vortices and anomalies, and their importance depends on the complexity and aperiodicity of the perturbation patterns. Additional terms, analogous to the fourth and sixth terms, would appear if the anomalies were partitioned into three or more levels rather than just two, but the interpretations would remain the same.

Equation (3.7) is the equation of piecewise tendency diagnosis (PTD), as applied to the intensification of an upper-level mobile trough. An analogous assemblage of terms, with the upper- and lower-level variables interchanged, could be used to study the development of a surface cyclone.

An equation such as (3.7) is appropriate for diagnosing the intensification of a particular PV anomaly, but what if one is interested in diagnosing the intensification of a particular height anomaly, such as the complete surface cyclone, which in general represents a superposition of two or more distinct PV anomalies at distinct levels? We propose the following multistage process for piecewise tendency diagnosis: 1) examine and invert the PV fields to identify the anomalies associated with the feature of interest; 2) select an appropriate partitioning strategy, such as upper level versus lower level and large scale versus small scale; 3) compute the contributions of individual PV anomalies to the overall intensity of the feature of interest; 4) apply (3.7) or its analog to the intensification of each important PV anomaly or height anomaly; and 5) examine the piecewise winds and advection patterns to check the dynamical interpretation of the piecewise tendencies. To this point, we have emphasized the quantitative aspects of the technique; qualitative interpretation of PV advection and associated dynamical processes have been discussed extensively elsewhere. *But unless one carefully examines the PV fields, the heights and winds associated with the PV anomalies, and the PV advection associated with those winds, one can only guess which dynamical processes are being quantitatively diagnosed with PTD.*

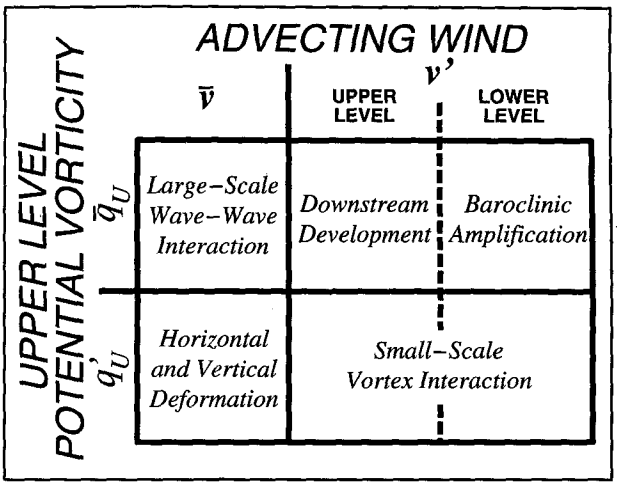

FIG. 4. Upper-level height tendency forcing terms in (3.7), showing basic dynamical interpretation of each term. See text for details.

4. Data and methods

a. Data source

This study uses Northern Hemisphere data from the National Meteorological Center (NMC) final analyses (Dey 1989; Kanamitsu 1989), which were prepared using 12 vertical levels and an R24 rhomboidal spherical harmonic truncation. The data were stored as 12-h global analyses on a 2.5° by 2.5° latitude–longitude grid at ten pressure levels between 1000 mb and 100 mb at the National Center for Atmospheric Research (NCAR).

The specific mobile trough used in this case study was one of the 27 469 mobile troughs identified and tracked in the 20-yr climatology of Lefevre and Nielsen-Gammon (1995). It formed on 1 December 1980 over the west coast of North America, moved across the United States, and formed a cutoff cyclone off the East Coast within a few days of its birth. This particular trough was selected because it intensified rapidly over a data-rich area of the Northern Hemisphere within a fairly straight zonal jet, so that a diagnosis (such as

PTD) would be expected to yield robust information. Although the objective algorithm tracked the trough for 21 days, making it one of the two longest-lived troughs to form in the area, only the first 4 days of the trough's life span are investigated here.

b. *Specification of a basic state*

By analogy with the simple dynamical models discussed in section 3, the atmospheric fields must be separated into large-scale and small-scale components. The small-scale fields should encompass the evolving synoptic-scale waves, and the large-scale fields should represent the basic-state medium within which the waves are embedded. Climatological-mean or zonal-mean basic states often bear little resemblance to the environments of synoptic-scale systems, which tend to follow tracks determined by the planetary-scale waves in the jet stream. Within a given segment of the jet stream, the alongstream average potential vorticity gradient is concentrated at the tropopause and is confined to a narrow horizontal band where the tropopause is vertical within the jet (Palmén and Newton 1948; Morgan 1994).

The most commonly used basic state for piecewise potential vorticity inversion of observed flows is a time-mean basic state, where the mean is computed over an interval long enough to encompass at least one period of the waves of interest (Davis and Emanuel 1991; Davis 1992a; Davis 1992b). This method is particularly useful for limited-area domains, but can cause difficulties when the waves are not periodic or the large-scale flow evolves during the averaging period.

Here, we adopt a spherical harmonic wavenumber truncation, whereby the basic state is composed of long waves and the perturbation is composed of short waves. The optimal truncation would be the largest wavenumber that avoids any projection of the mobile trough onto the large-scale fields. Based on inspection of individual maps with various truncations, we selected a maximum zonal wavenumber of 6 and a maximum total wavenumber of 9 for the large-scale fields. Blackmon (1976) also defined zonal wavenumbers 0–6 as large scale and found that those wavenumbers encompassed most of the 500-mb low-frequency variance. The higher total wavenumber maximizes the cross-jet structure of the basic state. The resulting total, large-scale, and small-scale height fields are shown in Fig. 5 at two times during the evolution of the mobile trough. Although the truncation is held fixed throughout the case study, the basic state evolves through the period as the long waves change amplitude and position. However, a reasonably clean separation between the mobile troughs and the large-scale field is maintained. Also, the minimum height within the trough agreed reasonably well with subjective measures of trough intensity.

The importance of the basic state should not be underestimated. The success of the PTD approach, as it is described here, relies on using the central value of perturbation height as a measure of the intensity of the disturbance of interest. If the choice of basic state does not adequately isolate the system from larger-scale features, the change in central height or central pressure will not correspond to the intensification or weakening of the system.

c. *Inversion of quasigeostrophic potential vorticity*

The mathematical details of the inversion procedure may be found in the appendix; a brief summary is given here.

Inversion of the system (2.2–2.3) requires the specification of q in the interior of the domain and θ along the upper and lower boundaries. Because the 1000-mb temperatures and heights in the analyses were found to be hydrostatically inconsistent in high terrain areas, mean temperatures were computed from the 850–1000-mb thickness and assigned to the midpoint of the layer with respect to $\ln p$, 922 mb. Using cubic splines, the height data were then interpolated to evenly spaced vertical levels with 100-mb resolution and the temperature analyses were interpolated to intermediate vertical levels. The stratification term in the definition of q [(2.1)] was then computed, and the stratification term and the geopotential height were transformed into spherical harmonic coefficients and the vorticity and potential vorticity computed. To avoid further vertical interpolation, all case study maps (below) are presented on the pressure levels used in the computation and inversion of potential vorticity.

For performing the inversion of QGPV using the system (2.2–2.3), we follow a numerical method similar to Holopainen and Kaurola (1991) and described in the appendix. Piecewise inversion and spatial filtering was performed by setting the spherical harmonic coefficients of QGPV at certain levels or wavenumbers to zero. Based on the vertical structure of the PV fields, upper levels are defined as 472 mb and above, and lower levels are defined as 572 mb and below. Note that our practice of setting QGPV to zero at certain levels for piecewise inversion follows Davis's technique (e.g., Davis and Emanuel 1991) rather than Holopainen and Kaurola's (1991) technique (see also Davis 1993; Holopainen and Kaurola 1993). The tendency inversion (2.7–2.8) uses the same inversion operator and proceeds in an analogous manner.

An alternative to the partitioning of q into upper and lower layers, which considers individual potential vorticity anomalies to be distinct entities, treats them as vortices. For example, an upper-level mobile trough might be defined as the positive anomalous small-scale potential vorticity in the core of the trough. This approach has been used by Hakim et al. (1996) on upper-level troughs and by Whitaker and Davis (1994) on diabatically generated potential vorticity anomalies. The vortex approach works well for isolated anomalies

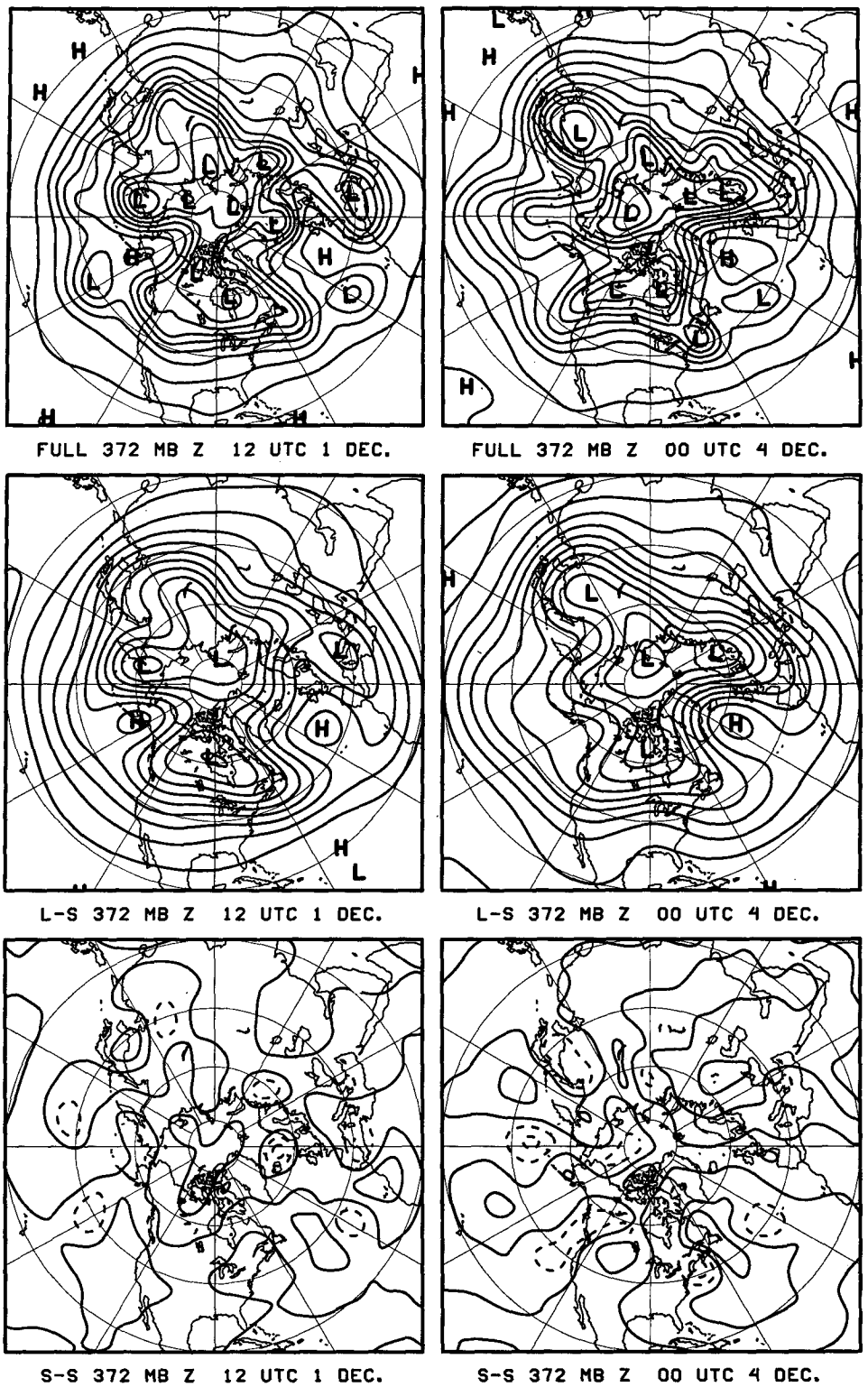

FIG. 5. Geopotential heights, 1200 UTC 1 December 1980 and 1200 UTC 3 December 1980. Top row: full heights, contour interval 12 dam. Middle row: large-scale heights, contour interval 12 dam. Bottom row: small-scale heights, contour interval 12 dam beginning at ±6 dam, negative contours dashed.

but is problematic when dealing with phenomena such as Rossby waves. When the anomaly field is periodic, the presence of a positive anomaly implies the existence of adjacent negative anomalies that are fundamentally part of the same dynamical entity and that cancel the effects of the positive anomaly at large distances.

5. Results

a. Overview of trough genesis

This section presents an overview of the evolution of heights and potential vorticity at upper and lower levels during the first four days of the mobile trough. To allow direct comparison with the diagnostic calculations, heights are shown at 372 mb and 872 mb (Figs. 6 and 7), rather than standard pressure levels.

The trough forms during 1 December 1980 over the Pacific Northwest, downstream of a larger-scale, stationary trough over the Gulf of Alaska. The wave in the q field rapidly amplifies during the next two days, eventually becoming nearly cut off from the reservoir of high q air over Canada by 1200 UTC 3 December. The perturbation height field also amplifies during this time, reaching a maximum amplitude of 372 m at 1200 UTC 3 December. According to the time series of perturbation heights (thick line in Fig. 8), the trough intensified most rapidly near 0000 UTC 2 December and filled most rapidly near 0000 UTC 4 December. (Because the trough formed within a narrow band of negative small-scale heights, the initial height value at 0000 UTC 1 December in the center of the trough is already significantly negative.)

The quasigeostrophic potential vorticity anomaly, although apparently evolving as a wave, developed closed contours and a maximum value of q greater than 5×10^{-5} s^{-1} as early as 0000 UTC 2 December. Such high values of q were not present initially, and this nonconservation of q is likely to be due to a combination of two adiabatic (Ertel PV-conserving) processes: the breakdown of geostrophic balance as the flow develops cyclonic curvature, and the lowering of the tropopause as the trough intensifies. These particular processes would tend to cause the quasigeostrophic diagnosis to underestimate the magnitude of intensification of the upper-level height anomaly.

The 1000–850-mb thickness (Fig. 7) shows that cold air is plunging southward east of the Rocky Mountains, while the upper-level trough deepens and moves eastward. A thermal wave forms along the thickness gradient at 0000 UTC 2 December and intensifies during the following two days. During 4 December, the cyclone occludes and becomes nearly vertical with the upper-level trough.

The close correspondence between positions of the q wave and upper-level trough suggests that the mobile trough is "induced" primarily by the upper-level q field. Bell and Bosart (1993) obtained a similar result for an upper-level cutoff cyclone. However, upper-level heights are also affected by low-level PV and surface potential temperature, and during the latter half of the period the low-level thermal wave and diabatically induced low-level PV anomaly also contribute to the intensity of the upper-level trough. Figure 9 compares the 372-mb height fields induced by the upper small-scale QGPV (φ'_U), heights induced by the lower small-scale QGPV (φ'_L), and the total 372-mb small-scale height field (φ') for 1200 UTC 2 December. At this time, the φ'_U low is much stronger than the φ'_L low (central heights of -280 m versus -50 m), and the heights associated with q'_U (in Fig. 9b) are almost indistinguishable from the total perturbation height field (in Fig. 9a). The total perturbation height field φ' is the sum of φ'_U and φ'_L, and the central value of the height minimum, which is -285 m, consists of about -280 m from φ'_U and about -5 m from φ'_L.

The amount by which the total height minimum deviates, in space and magnitude, from the minimum associated with the upper q' depends on the position and strength of the lower q' anomaly. Figure 8 shows the evolution of the small-scale height minima associated with q'_U, q'_L, and the full q', as well as the values of φ'_U and φ'_L at the location of the φ' minimum. Both the upper and lower centers reach maximum intensity at 1200 UTC 3 December, but the height perturbation at 372 mb induced by q'_L remains much weaker than the 372-mb height center induced by q'_U. This finding is consistent with the expectation that upper-level heights would be influenced more by the PV anomalies at upper levels than by the more distant PV anomalies at lower levels (Davis and Emanuel 1991). The q'_U height minimum deviates in value from the full perturbation height minimum during the latter half of the period, as the q'_L anomaly strengthens and the tilt between the upper and lower q' anomalies decreases.

According to Fig. 8, while φ'_U deepened by 21 dam (from -12 to -33 dam) between 1200 UTC 1 December and 1200 UTC 3 December, the overall height minimum φ' deepened by 26 dam (from -11 to -37 dam) during the same period. The additional 5 dam of intensification (about 20% of the total change in intensity) is due to heights induced by the low-level anomaly. At 1200 UTC 1 December, the value of φ'_L at the trough was $+1$ dam, while by 1200 UTC 3 December, it had dropped to -4 dam.

The drop in heights associated with φ'_L was due to a combination of superposition and amplification of the low-level anomaly. Quantitative evidence of superposition is contained in Fig. 8; for sinusoidal perturbations, the cosine of the phase shift between the upper trough and the height minimum induced by the lower wave is equal to φ'_L at the trough (the thin black dotted line) divided by the minimum value of φ'_L (the thin black solid line). At 1200 UTC 1 December, the vertical phase shift was greater than 90°, while by 1200 UTC

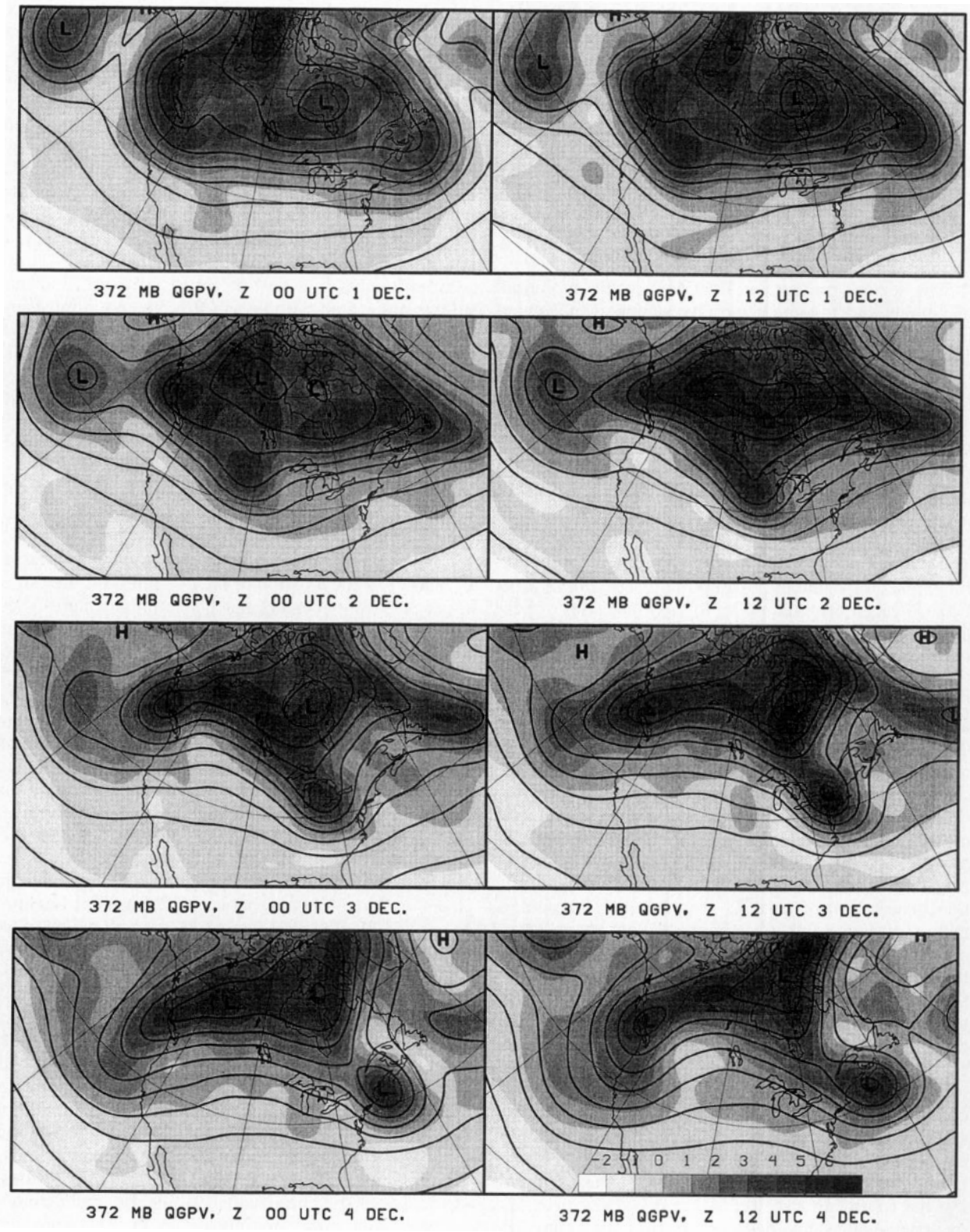

FIG. 6. The 372-mb quasigeostrophic potential vorticity (10^{-4} s^{-1}; color table at lower right), and geopotential heights (contour interval 12 dam).

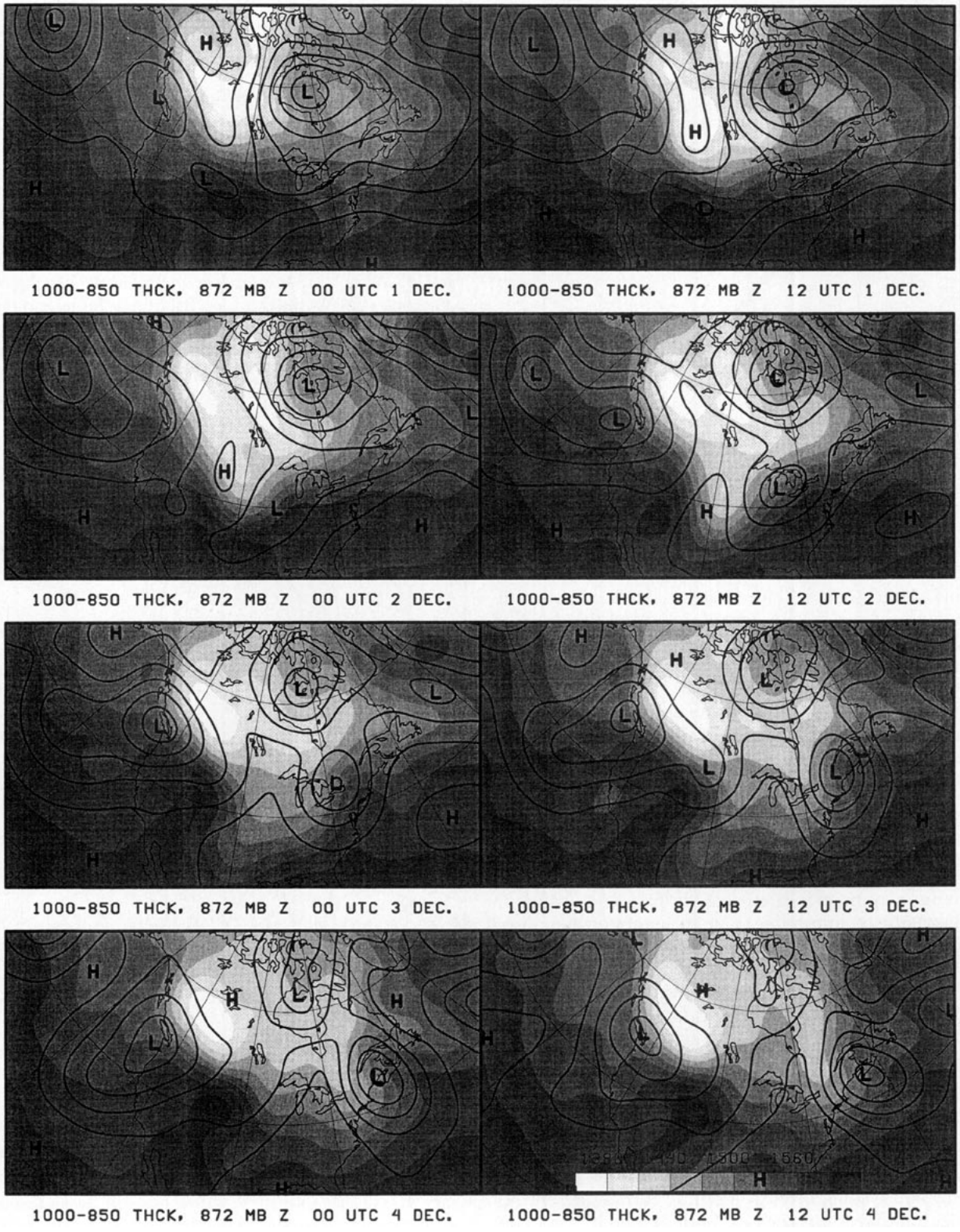

FIG. 7. 1000–850-mb thickness (m; color table at lower right), and 872-mb geopotential heights (contour interval 6 dam).

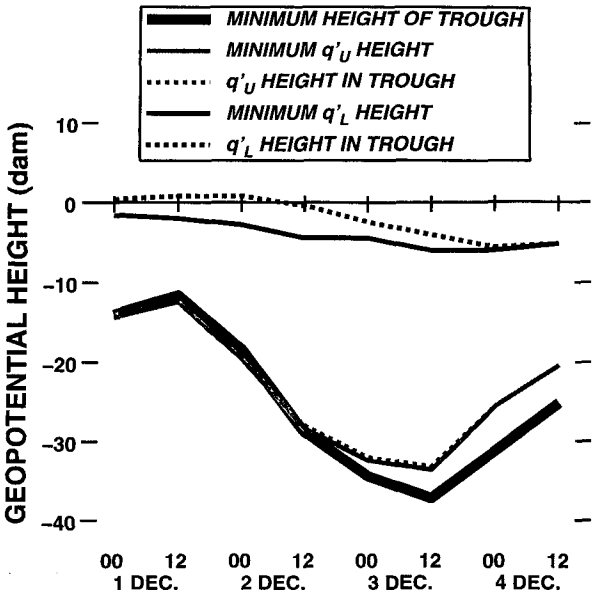

FIG. 8. Time series of geopotential heights associated with the upper-level trough and surface cyclone. See text for explanation.

3 December, the vertical phase shift was less than 45° and would soon become nearly zero. A complete diagnosis of the system, which is beyond the scope of this paper, would quantify the importance of superposition and amplification and would diagnose the dynamical causes of the low-level amplification. We shall focus on the intensification of the upper-level PV anomaly and its associated height field, which accounts for about 80% of the strengthening of the observed upper-level height perturbation.

b. Accuracy of quasigeostrophic tendencies

The rate of intensification of the upper height minimum may be measured directly from the change in the analyzed minimum value of height or diagnosed from the quasigeostrophic tendency at the location of the upper height minimum. The two tendencies, shown in Fig. 10, are similar in form, with intensification early and weakening late. Starting at 1200 UTC 2 December, the quasigeostrophic tendencies show less deepening, or more filling, than the actual tendencies. The largest difference is at 0000 UTC 3 December, when the quasigeostrophic diagnosis indicates the start of filling while in reality the deepening continues. Possible reasons for the discrepancy include the inherent inaccuracy of the quasigeostrophic system, discussed briefly earlier, and the neglect of diabatic processes, both of which should become more important later in the life cycle of the trough/cyclone system. The spatial patterns of diagnosed and actual tendencies over the Northern Hemisphere are also similar in position and magnitude (Lefevre 1995). We conclude that the quasigeostrophic diagnosis is adequate for examining the gross aspects of the adiabatic intensification of the mobile trough.

A similar comparison of intensification rates at 872 mb (not shown) indicates a systematic overestimate of the deepening by the quasigeostrophic equations after 0000 UTC 2 December of about 30 m/12 h, an amount comparable to the actual deepening rate of the 872-mb cyclone. This is somewhat surprising, since latent heating (a neglected process) would be expected to contribute strongly to low-level height falls. Ongoing analyses of other cyclones using the nonlinear balance equations suggest that surface friction is large enough to account for the observed discrepancy. The adiabatic, frictionless diagnosis of the 872-mb cyclogenesis must therefore be viewed with caution and used for qualitative purposes only.

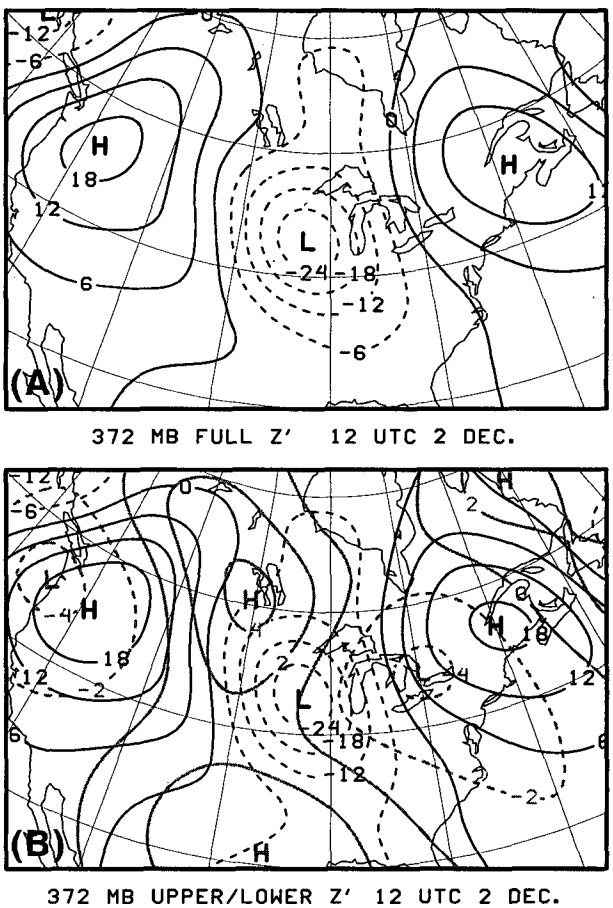

FIG. 9. (a) Full small-scale 372-mb geopotential heights (dam). (b) Small-scale 372-mb geopotential heights obtained by inverting upper-level potential vorticity (black, dam) and small-scale 372-mb geopotential heights obtained by inverting lower-level potential vorticity and surface potential temperature (gray, dam). The full small-scale height field (a) is the sum of the two height fields shown in (b).

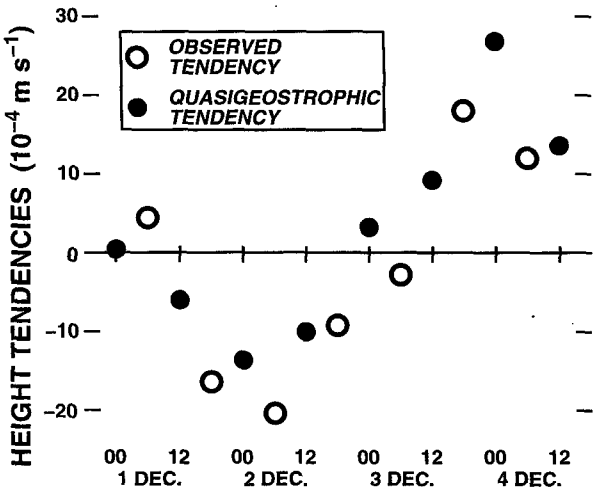

FIG. 10. Comparison of observed intensification of trough associated with upper-level small-scale potential vorticity (open circles; computed as a 12-h finite difference of minimum heights) with intensification rate computed from the quasigeostrophic height tendency equation (3.7) (filled circles; defined as instantaneous height tendency at location of minimum height).

c. *Piecewise diagnosis*

In the following sections, each of the dynamical processes is considered individually. Afterwards, the contributions of the various processes to the life cycle of the mobile trough are discussed.

1) DOWNSTREAM DEVELOPMENT

The dominant piecewise tendency term in (3.7) during the four days of study is $\pounds^{-1}(-\mathbf{v}'_U \cdot \nabla \bar{q}_U)'$, the advection of large-scale potential vorticity by the winds associated with the upper-level PV anomalies. This term contributes to development during the first two days and to weakening during the next two days.

In section 3, we showed that this term would contribute to development at the leading edge of a Rossby wave packet and can be interpreted as representing the propagation of Rossby wave energy. While recognizing that concepts such as Rossby waves must be defined broadly to be applied to the rapidly changing structure of the upper troposphere on these scales, we now explore that interpretation at two representative times in the life cycle of the upper-level trough.

At 1200 UTC 1 December, the intensification rate due to this term is largest. The q'_U anomalies and their induced small-scale circulation centers (Fig. 11a) are very nearly collocated, but the asymmetries and deviations from collocation are directly related to amplification or weakening of the q'_U anomalies. In particular, the winds around the q' anomaly of interest, over the northwestern United States near the center of the figure, are very asymmetrical, with strong positive $\bar{q}$ advection near and to the west of the anomaly and weak negative advection to the east of the anomaly. According to this advection pattern, the positive q' anomaly would indeed be intensifying.

The asymmetric forcing produces a corresponding asymmetric response in the height tendencies (Fig. 11b). The positive advection of $\bar{q}$ west of the trough is associated with large height falls, while the weak negative $\bar{q}$ advection east of the trough is associated with small height rises. Thus, a net height fall exists at the center of the trough, implying intensification. This pattern can also be interpreted as a trough fracture signature, with height rises induced between the developing trough and the preexisting upstream PV anomaly to its northwest (L. Bosart 1996, personal communication).

The asymmetric wind field is related to the asymmetric perturbation PV distribution. To the west of the trough is a strong negative small-scale PV anomaly that has no counterpart to the east of the trough. The negative and positive anomalies combine to yield strong northerlies, while only weak southerlies may be found to the east. The east–west variation in the strength of the $\bar{q}$ gradient also makes a minor contribution to the advection asymmetry. If the PV anomalies in the east–west chain had been equal in amplitude, the positive $\bar{q}$ advection (and height falls) west of the trough would have exactly equaled the negative $\bar{q}$ advection (and height rises) east of the trough, and the trough would simply have propagated westward by this mechanism.

A similar situation applies to the upstream ridge (the negative anomaly just off the Pacific coast): to its west is a strong positive anomaly, while to its east the positive anomaly is still weak. The southerlies to the ridge's west are stronger than the northerlies to the ridge's east, and since the southerlies are partly in phase with the negative q' anomaly, that anomaly should also be strengthened by this process. Although the basic-state QGPV gradient is far from uniform, the overall pattern seems analogous to the propagation of Rossby wave energy, with the east–west variations in the strength of PV anomalies leading to the local growth of wave crests and troughs.

Two days later, the same term is diagnosed as weakening the upper-level trough. The potential vorticity and winds (Fig. 12a) show that the trough, now situated over the eastern United States, is upstream of a strong negative PV anomaly. The southerlies associated with the trough and downstream ridge are considerably stronger than the northerlies upstream of the trough, and, in fact, the southerlies are partly in phase with the q' anomaly itself. Negative PV advection at the center of a positive PV anomaly would act to weaken the anomaly, and the tendency diagnosis (Fig. 12b) shows that the advection is acting to weaken the height perturbation as well.

The above interpretation, of wave energy being transported into the trough early in its life cycle and out of the trough later in its life cycle, is similar to the description of downstream baroclinic development

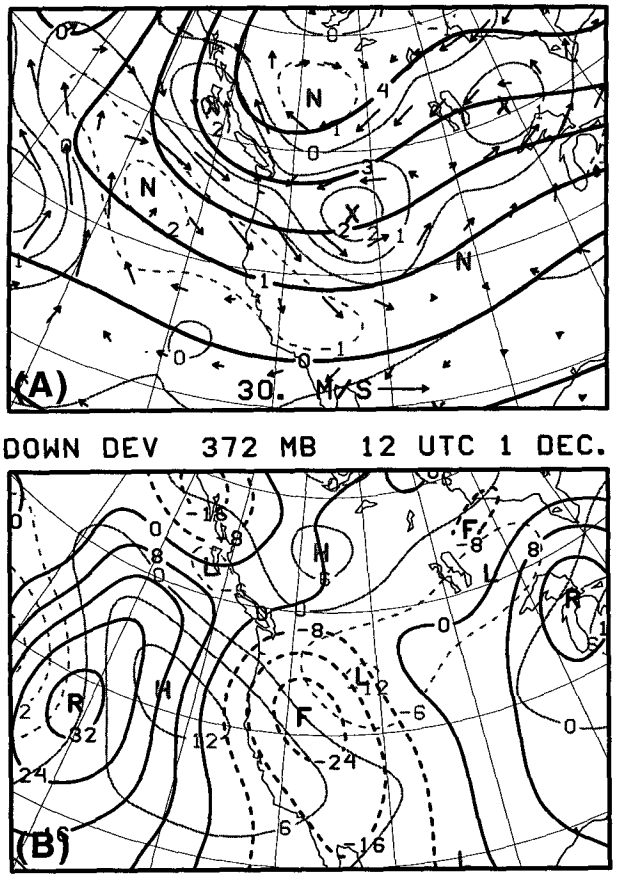

FIG. 11. Advections and tendencies associated with downstream development at 1200 UTC 1 December 1980. (a) Large-scale 372-mb potential vorticity (black, $\times 10^{-4}$ s^{-1}), small-scale 372-mb potential vorticity (gray, $\times 10^{-4}$ s^{-1}), and 372-mb winds associated with upper-level small-scale potential vorticity. (b) Small-scale 372-mb height tendencies associated with advection of upper-level large-scale potential vorticity by winds associated with upper-level small-scale potential vorticity (black, $\times 10^{-4}$ m s^{-1}; approximately equal to meters per three hours), and 372-mb heights associated with upper-level small-scale potential vorticity (gray, dam).

given by Orlanski and Katzfey (1991) and Orlanski and Chang (1993). However, their diagnosis was based on energy generation and transport, estimated using ageostrophic fluxes and flux convergence. In order to qualitatively compare our diagnosis to theirs, we have computed and plotted in Fig. 13 the horizontal components of the kinetic energy diagnostic used by Orlanski and Sheldon (1993; see also Chang and Orlanski 1994), which is the sum of the kinetic energy flux and the horizontal ageostrophic geopotential flux. The convergence of these flux vectors corresponds to the generation of kinetic energy, and net convergence within a volume encompassing the trough would correspond to intensification of the trough. The fluxes and flux convergences are consistent with the PV interpretation: energy is being transported downstream into the region of the developing trough at 1200 UTC 1 December and is being transported downstream out of the now strong trough at 1200 UTC 3 December. Comparisons at other times (not shown) between the height tendency due to basic-state PV advection by upper-level small-scale winds and the magnitude and sign of the energy flux convergence confirm that the two diagnostics agree both in sign and in relative magnitude throughout the 4-day period under diagnosis.

The upper-level transport of wave energy is only one aspect of downstream baroclinic development. We shall give a more complete discussion below.

2) BAROCLINIC AMPLIFICATION

The baroclinic amplification term, $\pounds^{-1}(-\mathbf{v}'_L \cdot \nabla \bar{q}_U)'$, was discussed in section 3c. It is similar in form to the downstream development term. Indeed, the interpretation of both of these terms depends critically on the structure of the basic-state effective PV gradients. If the effective PV gradient did not change sign between the lower and upper layers, the so-called baroclinic amplification term would actually represent vertical propagation of Rossby waves. Conversely, if the PV gra-

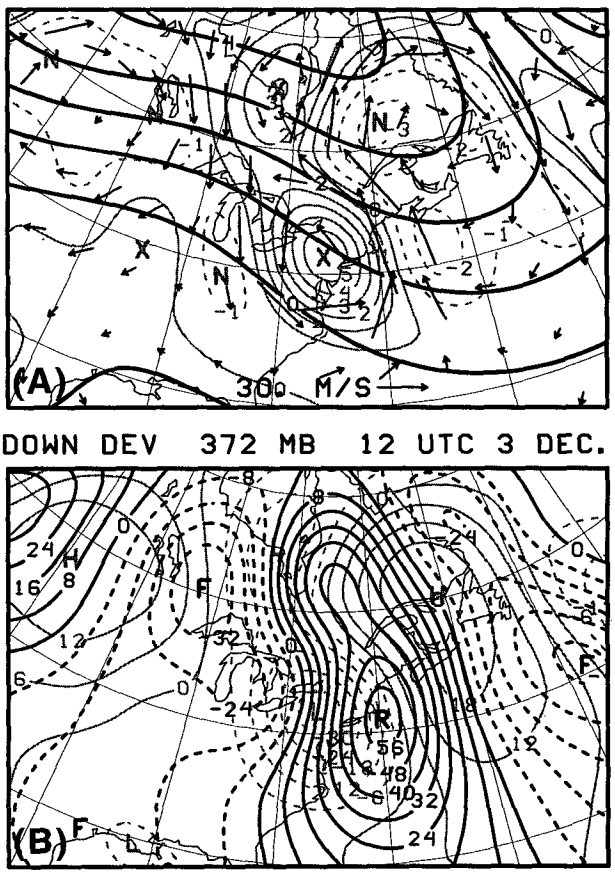

FIG. 12. Advections and tendencies associated with downstream development, as in Fig. 11, but for 1200 UTC 3 December 1980.

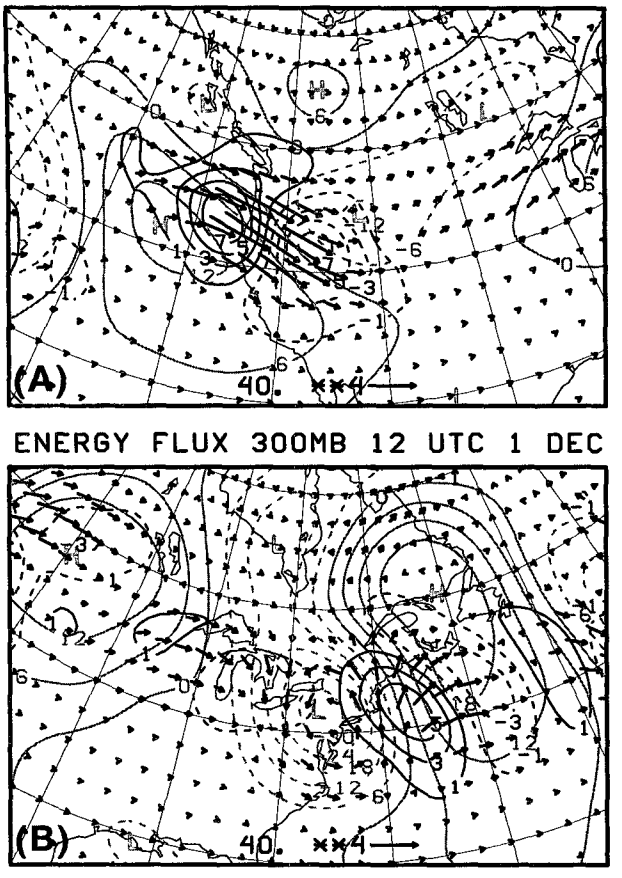

FIG. 13. Horizontal energy flux and flux divergence, following Orlanski and Sheldon (1993), for times shown in Figs. 11 and 12. Reference flux vector is 40×10^{-4} m^3 s^{-3}, flux divergence (black, contoured in intervals of 2×10^2 m^2 s^{-3}, negative values dashed), and 372-mb heights associated with upper-level small-scale potential vorticity (gray, dam, negative values dashed).

dient *did* change sign within the upper layer, the so-called downstream development term would also incorporate amplification due to barotropic instability.

Since the effective PV gradient is oppositely directed between upper and lower levels (cf. Figs. 6 and 7), the baroclinic amplification term should represent amplification (weakening) of the upper-level system due to a favorable (unfavorable) tilt between the upper and lower effective PV anomalies. Initially, the upper-level trough was upstream of cold air (and high pressure) at the surface along the Rocky Mountains (Figs. 6 and 7), but soon the trough moved into a favorable location between a surface cold air outbreak to its west and an intensifying frontal wave to its east. The baroclinic amplification term, which was inhibitory during 1 December, contributed to intensification starting 0000 UTC 2 December as the vertical tilt became favorable.

The advection pattern (372-mb winds associated with low-level q'/surface θ' overlaid on 372-mb $\bar{q}$) for 0000 UTC 3 December is plotted in Fig. 14a. Also shown is the q'_U field. The tilt between the upper-level trough (over the central United States) and the center of circulation associated with the low-level q' is nearly 90°, and as a result, the positive advection of upper-level $\bar{q}$ by the low-level-induced winds is almost exactly in phase with the existing q'_U anomaly, leading to amplification of the anomaly.

The height falls forced by this advection pattern (Fig. 14b) are likewise in phase with the upper-level trough. Note that although the winds associated with q'_L (Fig. 14a) are generally much weaker than the winds associated with q'_U (Fig. 11a), the favorable phase relationship means that the advection associated with q'_L primarily serves to intensify the trough, while most of the advection associated with q'_U is "wasted" on propagating the trough westward.

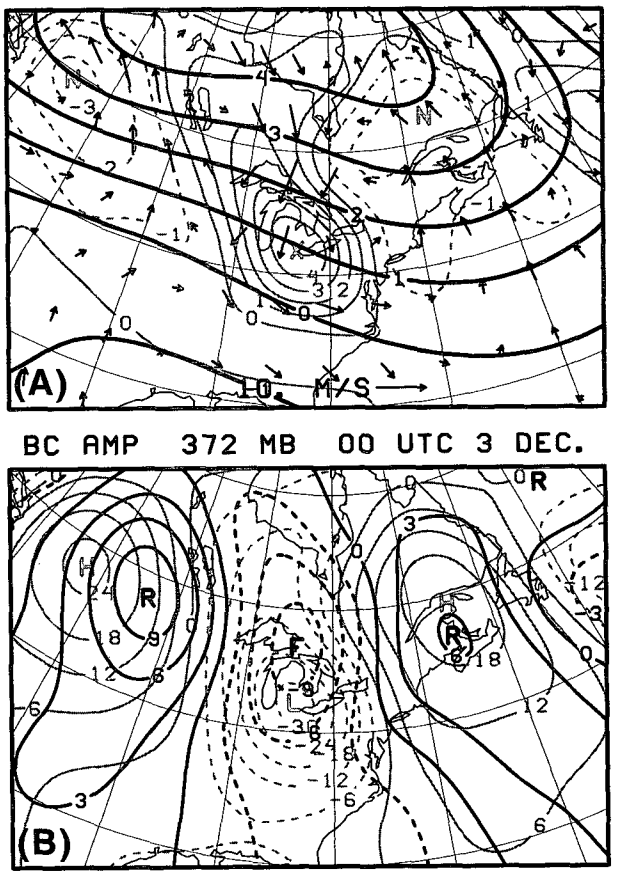

FIG. 14. Advections and tendencies associated with baroclinic amplification at 0000 UTC 3 December 1980. (a) Large-scale 372-mb potential vorticity (black, $\times 10^{-4}$ s^{-1}), small-scale 372-mb potential vorticity (gray, $\times 10^{-4}$ s^{-1}), and 372-mb winds associated with *lower*-level small-scale potential vorticity. (b) Small-scale 372-mb height tendencies associated with advection of upper-level large-scale potential vorticity by winds associated with lower-level small-scale potential vorticity (black, $\times 10^{-4}$ m s^{-1}), and 372-mb heights associated with upper-level small-scale potential vorticity (gray, dam).

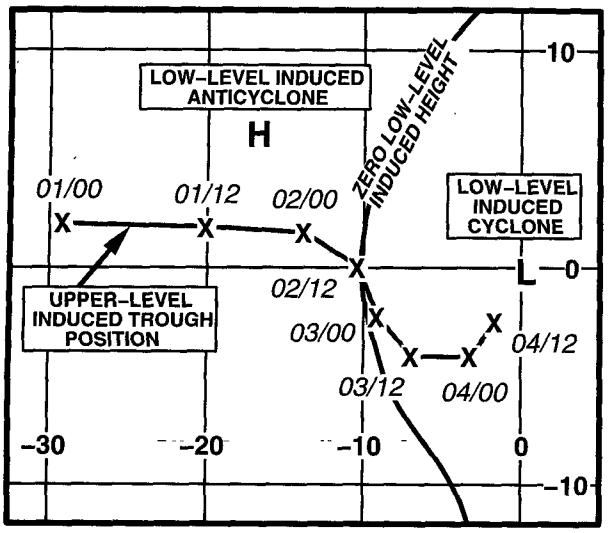

FIG. 15. Semischematic depiction of position of the trough associated with upper-level small-scale potential vorticity relative to the high–low couplet associated with low-level small-scale potential vorticity (including surface potential temperature). Latitudes and longitudes are shown relative to the low-level cyclone induced by low-level small-scale potential vorticity. Dates and times are given as day/hour UTC. The position of the $Z = 0$ contour from the inversion of low-level small-scale potential vorticity is also shown.

The tilt between the upper and lower systems decreased steadily until 0000 UTC 4 December, when the system became nearly vertical and intensification ceased. The position of the trough induced by upper-level q relative to the heights induced by the surface θ' and lower-level q' is shown semischematically in Fig. 15 for the period 1–4 December. The relative motion of the trough is reminiscent of the progression shown by Sanders (1986, his Fig. 12) for 500-mb vorticity centers and rapidly deepening surface cyclones along the east coast of North America. The rapid relative motion of the upper-level trough during the first day and slower motion during the following two days is consistent with its phase relationship with the low-level q/θ pattern: while upshear of the low-level high, the winds induced by low levels act to speed the wave to the east; while downshear of the low-level high, the winds induced by low levels act to slow the wave down. This interaction is mutual; relative to the earth, the upper-level wave moved fastest and the lower-level wave moved slowest during the first day. The upper and lower waves never quite "phase locked" (Hoskins et al. 1985), and when the relative east–west motion was slowest, the upper-level q anomaly was being advected southward by the winds associated with the low-level cyclone. This sort of nonlinear advection suggests that true phase locking may be difficult to accomplish in the atmosphere with typical finite-amplitude systems: even if upper and lower systems maintain a nearly constant horizontal separation, as in Grotjahn and Tribbia (1995), their induced winds should cause them to rotate counterclockwise around each other.

The maximum intensification rate due to baroclinic amplification was not at 1200 UTC 2 December, when the trough was most nearly 90° out of phase with the surface system, but instead occurred during the following 24 h. The lower-level frontal wave continued to amplify while the tilt became less favorable, and as a result the advection of upper-level $\bar{q}$ due to the lower-level wave became stronger.

In order to differentiate baroclinic amplification from the vertical propagation of Rossby waves, it is necessary to verify that the same process is leading to the growth (rather than the decay) of the lower-level wave. Certainly, if we are correct in our basic assumption that the important low-level effective PV gradient is the surface θ gradient, which is opposite in sign to the upper-level PV gradient, then a phase tilt conducive to baroclinic amplification at upper levels would also be conducive to baroclinic amplification at lower levels. Figure 16, the counterpart to Fig. 13a, shows that the winds associated with the upper-level small-scale QGPV are southerly near the thickness anomaly, producing warm advection and amplification of the anomaly. The associated height tendencies (not shown) confirm that $\mathcal{L}^{-1}(-\mathbf{v}'_U \cdot \nabla \bar{q}_L)'$ is responsible for the bulk of the diagnosed intensification of the low-level cyclone, that intensification due to baroclinic amplification occurs at upper and lower levels simultaneously, and that this intensification depends on the strength of the anomalies and the vertical tilt of the system. Incidentally, baroclinic amplification was strongest at low levels 12–24 h before it was strongest at upper levels. For an upper-level trough to amplify by this process, the low-level cyclone must first become sufficiently in-

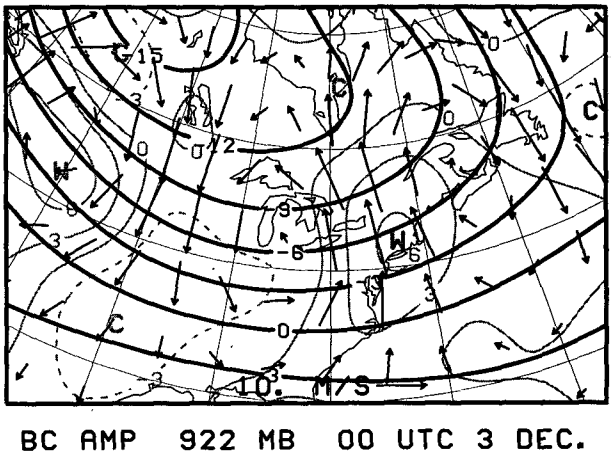

FIG. 16. Advections associated with baroclinic amplification of the low-level thermal wave, 0000 UTC 3 December 1980. (a) Large-scale 1000–850-mb thickness (black, dam), small-scale 1000–850-mb thickness (gray, dam), and 922-mb winds associated with *upper*-level small-scale potential vorticity.

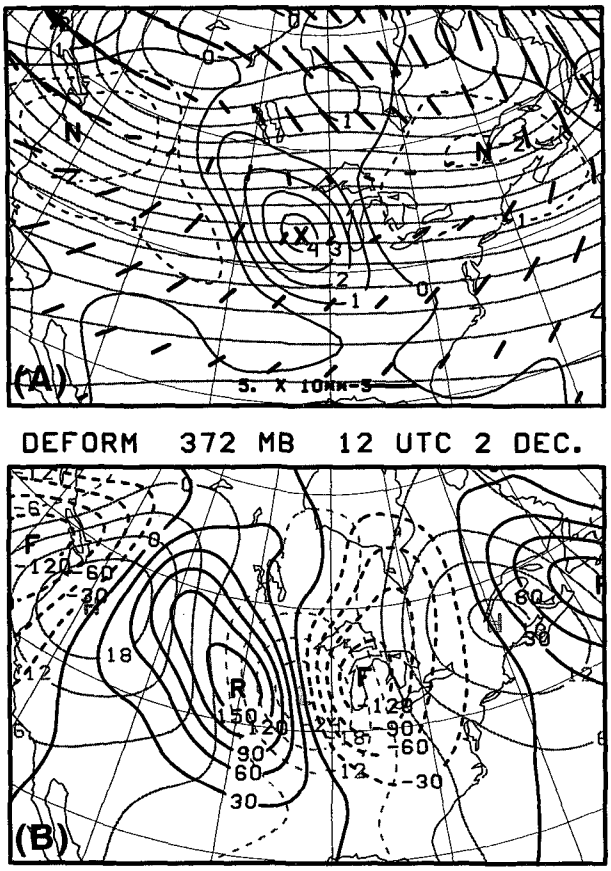

FIG. 17. Deformation and tendencies associated with large-scale upper-level flow at 1200 UTC 2 December 1980. (a) Small-scale 372-mb potential vorticity (black, $\times 10^{-4}$ s^{-1}), large-scale 372-mb heights (gray, contour interval 6 dam), and 372-mb axes of dilatation associated with large-scale deformation (lengths of axes are proportional to the local magnitude of deformation; scale at bottom is in s^{-1}). (b) Small-scale 372-mb height tendencies associated with advection of upper-level small-scale potential vorticity by large-scale winds (black, $\times 10^{-4}$ m s^{-1}), and 372-mb heights associated with upper-level small-scale potential vorticity (gray, dam).

tense to be able to induce strong advections at the level of the upper-level trough.

3) BAROTROPIC DEFORMATION

The deformation term, $\pounds^{-1}(-\bar{\mathbf{v}}\cdot\nabla q_U')'$, represents the third process that is important to the development of the upper-level mobile trough. Depending on the vertical structure of the upper-level anomaly, this term may involve not only horizontal (barotropic) deformation, as discussed in section 3c and studied by Farrell (1989b), but also vertical deformation by the basic-state vertical shear within upper levels, which was responsible for rapid initial growth in the system described in Farrell (1989a). In order to separate horizontal and vertical deformation effects, we set the large-scale wind field equal to the 372-mb large-scale wind field at all levels and computed the tendency by this vertically uniform wind. The difference between this barotropic deformation tendency and the full deformation tendency is attributed to vertical shear.

The barotropic deformation tendency was typically about three times as large as the vertical deformation tendency. Barotropic deformation contributed to intensification while the trough was amplifying, but acted to weaken the trough during 4 December while the trough was filling. The tendency field (Fig. 17) is dominated by a positive–negative couplet associated with the advection of the PV anomaly as a whole. The net tendency at the center of the trough, associated with slight horizontal variations in the basic-state wind field, cannot be discerned by eye.

To better understand the role of the variations in the background wind field, the deformation field associated with the large-scale wind is represented in Fig. 17a by axes of dilatation. At 1200 UTC 2 December, the elliptical q' anomaly is oriented northwest–southeast. In the central and southern portions of the anomaly, the axis of dilatation is oriented southwest–northeast, indicating that the large-scale winds are attempting to make the anomaly more circular and thereby increase the small-scale height perturbation, as discussed in section 3c.

At 0000 UTC 4 December (Fig. 18), the positive q' anomaly is more circular, but it is still somewhat elongated in the north–south direction. The axes of dilatation are generally oriented north–south as well, and the apparent angle of less than 45° between the major axis of the trough and the axis of dilatation is consistent with the large-scale flow acting to stretch out the q' anomaly and make the height perturbation weaker.

The vertical deformation term, by contrast, was associated with height rises during the early stages of development and height falls during the latter stages. Because these tendencies were comparatively small,

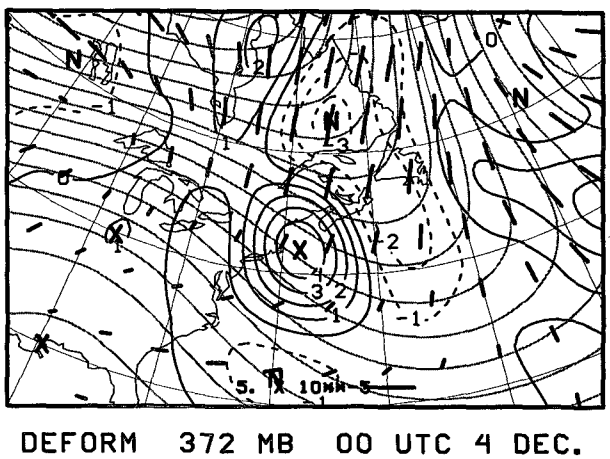

FIG. 18. Deformation associated with large-scale upper-level flow, as in Fig. 17a, but for 0000 UTC 4 December 1980.

the physical reasons for the variations in vertical tilt and shear that produced these tendencies will not be considered here.

4) VORTEX–VORTEX INTERACTION

The $\mathfrak{L}^{-1}(-\mathbf{v}'_U \cdot \nabla q'_U)'$ and $\mathfrak{L}^{-1}(-\mathbf{v}'_L \cdot \nabla q'_U)'$ terms in (3.7) represent the advection of small-scale QGPV by winds associated with the small-scale QGPV itself. The first term describes the interaction of adjacent q'_U anomalies as they reconfigure themselves or change their shapes. The second term tends to be much smaller and has been included with the first for convenience. It represents changes of shape or configuration of upper-level QGPV anomalies due to the winds induced by the lower-level anomalies. Together, the two terms may be written $\mathfrak{L}^{-1}(-\mathbf{v}' \cdot \nabla q'_U)'$.

The height tendencies due to these processes were generally weaker and more erratic than those due to the other processes discussed so far. The most important contribution from these terms came at the 0000 UTC 1 December, when the trough was just forming. At that time, vortex–vortex interaction made a larger contribution to trough intensification than any other process.

The 0000 UTC 1 December small-scale 372-mb QGPV and small-scale 372-mb winds are overlaid in Fig. 19a. To a first approximation, the small-scale winds are parallel to the q' contours, but the small deviations from this pattern are entirely responsible for the q' advection and associated height tendencies. The incipient trough is in the Pacific Northwest; to its immediate north and south are areas of negative q'. The induced winds are a bit "smoother" than the q' field; as a result of this smoothness and the configuration of q', the negative q' to the north is being advected northward away from the trough, while the negative q' to the south is being advected southeastward away from the trough. The direct effect of these advections would be an expansion in the north–south direction of the presently east–west oriented anomaly, with a resulting increase in the amplitude of its induced height field. The associated height tendencies (Fig. 19b) are mostly negative throughout the area of the incipient mobile trough, as a result of the predominantly positive q'_U advection.

This process was short-lived, though; by 1200 UTC 1 December (not shown), the QGPV anomaly was much more symmetrical and the local tendency due to the vortex–vortex interaction term had gone to zero.

5) NONLINEAR LARGE-SCALE WAVE–WAVE INTERACTIONS

The remaining forcing term in (3.7), $\mathfrak{L}^{-1}(-\bar{\mathbf{v}} \cdot \nabla \bar{q}_U)'$, represents the projection onto the small scale of the advection of large-scale QGPV by winds associated with the large-scale QGPV itself. This term was relatively small throughout the life cycle of the mobile trough, and

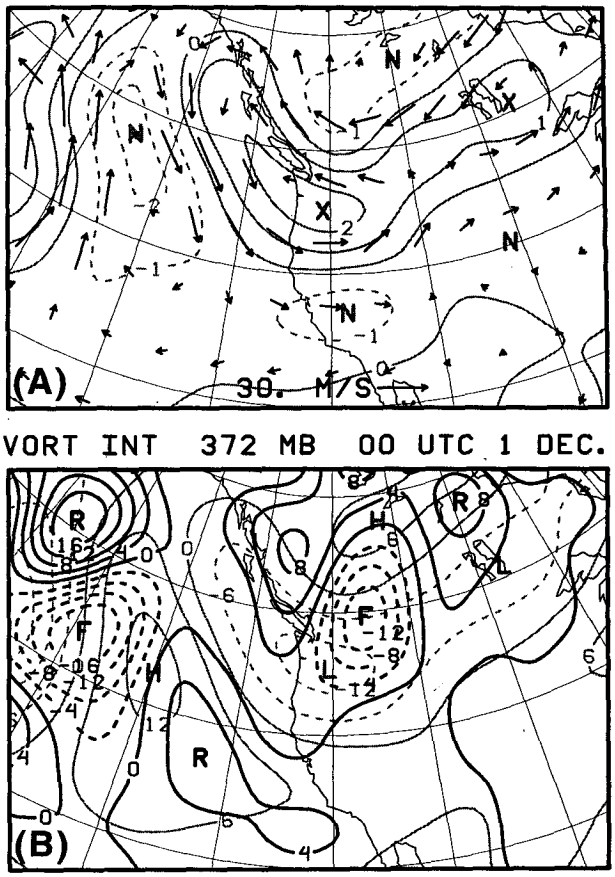

FIG. 19. Advections and tendencies associated with small-scale vortex interaction at 0000 UTC 1 December 1980. (a) Small-scale 372-mb potential vorticity (gray, $\times 10^{-4}$ s^{-1}), and 372-mb winds associated with upper-level small-scale potential vorticity. (b) Small-scale 372-mb height tendencies associated with advection of upper-level small-scale potential vorticity by winds associated with upper-level small-scale potential vorticity (black, $\times 10^{-4}$ m s^{-1}), and 372-mb heights associated with upper-level small-scale potential vorticity (gray, dam).

we would expect it to be small except where scale contraction of planetary waves is taking place.

d. The life cycle of trough growth and decay

The evolution of the dynamical contributions to the intensification or weakening of the upper-level trough during its life cycle is summarized in Fig. 20. All terms in (3.7) are plotted, so the sum of the terms equals the total quasigeostrophic tendency given in Fig. 8 and indicated by the filled circles in Fig. 20. Note that negative tendencies correspond to intensification of the mobile trough. As discussed earlier, the timing and magnitude of these changes were roughly consistent with the observed behavior of the mobile trough. While reading this discussion, refer back to Figs. 6 and 7, which show the upper-level and lower-level features at 12-h intervals. Also, recall that vertical superposition

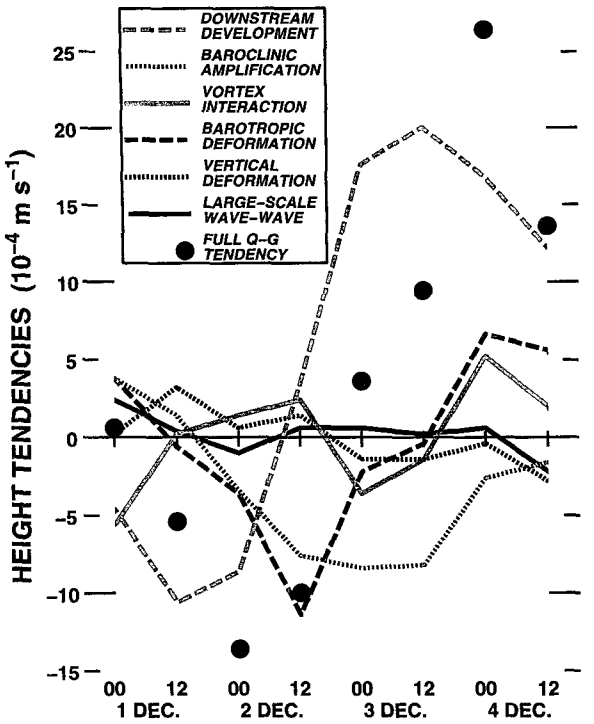

FIG. 20. Height tendencies associated with various dynamical processes during the development of the upper-level mobile trough, 0000 UTC 1 December 1980 to 1200 UTC 4 December 1980. Also shown are the total quasigeostrophic tendencies (black circles), which are the sums of the individual tendencies.

and low-level amplification caused the total perturbation heights to fall an additional 5 dam in two days, an average rate of -3×10^{-4} m s^{-1}.

The trough was triggered at 0000 UTC 1 December by a combination of vortex–vortex interaction and downstream development. We regard the vortex–vortex interaction as a chance reorganization of small-scale PV anomalies, but the downstream development represents a sustained transport of wave energy from an upstream ridge and trough. At this early stage, the trough was upstream of a cold surface anticyclone, a configuration unfavorable for baroclinic development.

By 0000 UTC 2 December the trough had moved east of the surface anticyclone and had begun generating a frontal wave over the central United States. Also because of this change in configuration, the winds associated with the surface cold anomaly and developing warm anomaly helped to amplify the upper-level trough itself. This baroclinic amplification increased as the surface cyclone intensified and would become the primary contributor to height falls by 0000 UTC 3 December. Baroclinic amplification remained a minor contributor to growth even after the cyclone occluded at 0000 UTC 4 December, as the system retained a slight upshear tilt.

The increase in strength of the mobile trough was also the primary cause of its eventual weakening. While the trough was weaker than its upstream counterparts, it received Rossby wave energy, but once the trough reached sufficient intensity, it became a net *source* of Rossby wave energy, radiating energy downstream. The downstream development term became unfavorable to growth at 1200 UTC 2 December, and by 3 December the weakening due to downstream development dominated all other processes and produced net weakening of the mobile trough.

This basic sequence of events (trough formation by downstream propagation of wave energy, generation of a surface frontal wave and trough growth by baroclinic amplification, loss of wave energy downstream even as baroclinic growth continues, and eventual weakening as baroclinic amplification ceases) mirrors the downstream baroclinic development process simulated by Simmons and Hoskins (1979) and described by Orlanski and Katzfey (1991) for a case of Southern Hemisphere cyclogenesis. The fundamental processes appear to be the initial growth of new cyclones by downstream propagation of wave energy from an upstream disturbance, followed by downstream propagation of energy away from the new cyclone as it continues to grow baroclinically and extract energy from the basic state. Chang and Orlanski (1993), in an idealized storm track simulation, likewise found a very similar evolution for a downstream eddy: initial growth by wave propagation, then baroclinic amplification, which was soon damped and overwhelmed by loss of energy by wave propagation. Since completely different diagnostic techniques were employed by Orlanski and coworkers and by the present study, the similarity of results suggests not only that both diagnostic techniques are valid and complementary, but also that the downstream development process is a common trigger of trough formation and subsequent cyclogenesis in midlatitudes.

Additional processes not explicitly included in downstream development also played significant roles during the life cycle of the mobile trough. The most important of the remaining processes was barotropic deformation, which helped to strengthen the trough during its growth phase and weaken the trough during its decay phase. We do not know whether this behavior is common to mobile troughs. However, the mobile trough genesis event analyzed by Nielsen-Gammon (1995) also was triggered by downstream development and subsequently amplified partly by barotropic large-scale deformation prior to surface cyclogenesis. The similarity of the two events suggests that deformation may be a frequent contributor to the intensification of mobile troughs early in their life cycles. Following occlusion, barotropic deformation acted to weaken the trough. We suspect that this is also a common occurrence: once a cutoff PV anomaly has formed, the background deformation should typically act to destroy the disturbance's symmetry and shear out the PV anomaly.

The remaining processes, as seen in Fig. 20, were weak and erratic and, with the possible exception of vortex–vortex interaction during the initiation of the mobile trough, were judged not to be significant to the growth and decay of the trough.

6. Concluding remarks

Upper-tropospheric mobile troughs are an ubiquitous feature of midlatitude flow and common precursors to surface cyclogenesis, but the process by which they form is largely unknown. Motivated by a desire to quantify "PV thinking" (Hoskins et al. 1985), we have developed a technique called piecewise tendency diagnosis, or PTD, and applied it to the development of an upper-tropospheric midlatitude mobile trough. The life cycle of the upper-level QGPV anomaly, from initial trough genesis to eventual formation of a cutoff, occluded cyclone, has been described quantitatively in terms of the specific dynamical processes contributing to development. The diagnosis, while more complete than previous case studies (Orlanski and Katzfey 1991; Orlanski and Sheldon 1993; Nielsen-Gammon 1995), found similar dynamical processes at work, including downstream development, baroclinic amplification, and large-scale deformation.

The analysis was made somewhat simpler by diagnosing only the heights associated with the upper-level QGPV anomaly; as seen in Fig. 8, the lower-level PV–θ field also contributes to the intensity of the 500-mb trough, especially late in its evolution. The tendency due to vertical superposition and low-level amplification is of the same sign as the baroclinic amplification term and one-half to one-third its magnitude at every time between 1200 UTC 1 December and 0000 UTC 4 December. Thus, while vertical superposition made a minor contribution to the intensity of the observed trough, most of the change in intensity was due to changes in the PV field at upper levels. This may often be the case for upper-level mobile troughs, but it appears to be generally not true for surface cyclones, for which vertical superposition of the upper-level PV anomaly seems to be a significant contributor to intensity (Davis and Emanuel 1991).

The PTD method may be extended in obvious ways to account for orographic and thermal forcing and latent heat release. To the extent that the integrated effect of these processes is manifested in the observed interior PV and surface temperature distribution, the effect of these processes is already partly diagnosed. The missing pieces represent, for example, height tendencies due to the ongoing generation of an interior PV dipole by latent heat release. Winds induced by the diabatic PV anomalies are already incorporated in PTD, although we do not distinguish them from the effects of PV anomalies produced adiabatically.

In summary, the PTD method appears to be a powerful technique for understanding synoptic-scale development. It is complementary to other techniques, such as omega equation diagnostics and local kinetic energy diagnostics, and is particularly suited to relating observed systems to theoretical paradigms of Rossby waves, baroclinic instability, and nonmodal growth.

Acknowledgments. We are grateful for comments and suggestions from Lance Bosart, Edmund Chang, Gary Lackmann, David Gold, Wayne Bresky, and Robert Black. The kinetic energy flux computations were performed by Matt Wandishin. This research was sponsored by the National Science Foundation under Grant ATM-9218306 and by the United States Air Force.

APPENDIX

Inversion Algorithms

The spherical harmonic expansion of a function such as geopotential height Z is defined as (see Washington and Parkinson 1986)

$$Z = \sum_{m=0}^{M} \sum_{n=m}^{N} (Z_n^m P_n^m(\mu) e^{im\lambda}), \qquad \text{(A.1)}$$

where λ is longitude, μ is sin(latitude), and $P_n^m(\mu)$ are the normalized associated Legendre polynomials:

$$P_n^m(\mu) = \left[\frac{(2n+1)(n-m)!}{2(n+m)!}\right]^{1/2}\left[\frac{(1-\mu^2)^{m/2}}{2^n n!}\right] \times \left[\frac{d^{(m+n)}}{d\mu^{(m+n)}}(\mu^2-1)^n\right]. \qquad \text{(A.2)}$$

With the gridded data available at mandatory levels on a 2.5° by 2.5° latitude–longitude grid, $M = N = 72$. All spherical harmonic transformations were performed using SPHEREPACK Version 1.1, written by John Adams and Paul Swarztrauber and available by anonymous FTP (ftp.ucar.edu) from the National Center for Atmospheric Research (NCAR). The large-scale field is given by all coefficients with ($m \leq 6$; $m + n \leq 9$); the small-scale field is given by the remaining coefficients. Since data was used only from the Northern Hemisphere, a symmetric distribution of height about the equator was assumed for calculating the coefficients.

The use of spherical harmonics simplifies the computation of vorticity, but the stratification term in (2.1) requires vertical finite differencing. To simplify this phase of the calculation, heights were interpolated vertically to evenly spaced pressure levels ($\Delta p = 100$ mb) from 872 mb to 172 mb using cubic splines (Press et al. 1992), and the vertical derivative of height, required for the boundary condition (2.3), was computed using centered difference with respect to $\ln p$ and assigned to 922 mb and 122 mb. The nonstandard pressure levels were chosen to allow direct application of the lower

boundary condition, computed from heights at 850 mb and 1000 mb.

In finite difference form, the spherical harmonic coefficients of the potential vorticity q (2.1) at a given vertical level k are determined from

$$
\begin{aligned}
(q_n^m)_k - f_n^m &= \left[\frac{gf_0}{(\Delta p)^2\sigma_{k-1/2}}\right](Z_n^m)_{k-1} \\
&\quad + \left[\frac{gf_0}{(\Delta p)^2\sigma_{k+1/2}}\right](Z_n^m)_{k+1} \\
&\quad - \left[\frac{g}{f_0}\left(\frac{-n(n+1)}{a^2}\right)\right. \\
&\quad \left. + \frac{gf_0}{(\Delta p)^2(\sigma_{k+1/2}+\sigma_{k-1/2})}\right](Z_n^m)_k \\
&= (A_n^m)_k(Z_n^m)_{k-1} + (B_n^m)_k(Z_n^m)_k \\
&\quad + (C_n^m)_k(Z_n^m)_{k+1}, \quad \text{(A.3)}
\end{aligned}
$$

where $a = 6.37 \times 10^6$ m is the radius of the earth and $f_0 = 1 \times 10^{-4}$ s^{-1} is the reference value of the Coriolis parameter f. At the lowest ($k = 1$) and highest ($k = 8$) levels, the application of the boundary conditions yields slightly different equations. For example,

$$
\begin{aligned}
&(q_n^m)_1 - f_n^m + \frac{gf_0}{\Delta p\sigma_{1/2}}\left(\frac{\partial Z}{\partial p}\right)_{1/2} \\
&\quad = \left[\frac{gf_0}{(\Delta p)^2\sigma_{3/2}}\right](Z_n^m)_2 \\
&\quad\quad - \left[\frac{g}{f_0}\left(\frac{-n(n+1)}{a^2}\right) + \frac{gf_0}{(\Delta p)^2\sigma_{3/2}}\right](Z_n^m)_1 \\
&\quad = (B_n^m)_1(Z_n^m)_1 + (C_n^m)_1(Z_n^m)_2. \quad \text{(A.4)}
\end{aligned}
$$

The system of eight equations for the potential vorticity coefficients at the eight pressure levels may be written

$$\mathbf{A_n^m Z_n^m} = \mathbf{q_n^{*m}}, \quad \text{(A.5)}$$

where the elements of $\mathbf{q_n^{*m}}$ are the left-hand sides of (A.3), (A.4), and the equation corresponding to (A.4) for $k = 8$, and $\mathbf{A_n^m}$ is an 8×8 tridiagonal matrix containing the coefficients $(A_n^m)_k$, $(B_n^m)_k$, and $(C_n^m)_k$.

To invert the potential vorticity field to obtain the height field, one solves (A.5) for $\mathbf{Z_n^m}$:

$$\mathbf{Z_n^m} = (\mathbf{A_n^m})^{-1}\mathbf{q_n^{*m}}, \quad \text{(A.6)}$$

using a standard tridiagonal solver routine (Press et al. 1992). To perform piecewise potential vorticity inversion, we set the appropriate elements of $\mathbf{q_n^{*m}}$ to zero before solving (A.6).

The QGPV height tendency equation is similar to (A.6):

$$\boldsymbol{\chi}_\mathbf{n}^\mathbf{m} = (\mathbf{A_n^m})^{-1}\mathbf{F_n^m}, \quad \text{(A.7)}$$

where the elements of $\boldsymbol{\chi}$ are the spherical harmonic coefficients of the height tendency $\partial Z/\partial t$ at each level and the forcing $\mathbf{F}$ is the advection of QGPV [along with advection of thickness $\partial Z/\partial p$ at the upper and lower boundaries; cf. (A.4)]. The forcing is computed using finite differences on the latitude–longitude grid.

Piecewise tendency computations use various elements of the forcing for the right-hand side of (A.7). For example, to compute the height tendency associated with the last forcing term in (3.7), $\pounds^{-1}(-\mathbf{v}_L' \cdot \nabla q_U')'$, we follow the following procedure: 1) obtain the spherical harmonic coefficients of q' by computing the spherical harmonic coefficients of q from (A.1) and (A.5) and setting all small-wavenumber coefficients ($m \leq 6$; $m + n \leq 9$) of q to zero; 2) set the upper-level values ($5 \leq k \leq 8$) of q' (and upper-boundary perturbation thickness) to zero, solve (A.6) for $(\mathbf{Z_L'})_\mathbf{n}^\mathbf{m}$, and compute the spherical harmonic coefficients of v_L'; 3) transform q' and v_L' from coefficients to gridpoint values and compute the advection of q' by v_L' at upper levels (and advection of upper boundary perturbation thickness); 4) transform the upper-level advection into spherical harmonic forcing coefficients $\mathbf{F_n^m}$, set all small-wavenumber coefficients to zero, and solve (A.7) for the height tendency; and 5) transform the filtered forcing and height tendency coefficients back to the latitude–longitude grid.

In order that height tendencies measure intensification rather than translation, the tendencies must be evaluated as close to the location of the height minima as possible. Simply finding the locally lowest-valued grid point is unsatisfactory. (For example, the gradient at such a point, computed using centered differences, will in general be nonzero.) For this study, the locations and magnitudes of perturbation height minima were found from the spherical harmonic height coefficients using the downhill simplex method (Press et al. 1992). Tendencies were then computed directly at those points from the spherical harmonic tendency coefficients.

REFERENCES

Bell, G. D., and L. W. Bosart, 1993: A case study diagnosis of the formation of an upper-level cutoff cyclonic circulation over the eastern United States. *Mon. Wea. Rev.*, **121,** 1635–1655.

Bishop, C. H., and A. J. Thorpe, 1994: Potential vorticity and the electrostatics analogy: Quasi-geostrophic theory. *Quart. J. Roy. Meteor. Soc.*, **120,** 713–731.

Blackmon, M. L., 1976: A climatological spectral study of the 500 mb geopotential height of the Northern Hemisphere. *J. Atmos. Sci.*, **33,** 1607–1623.

Bretherton, F. P., 1966: Critical layer instability in baroclinic flows. *Quart. J. Roy. Meteor. Soc.*, **92,** 325–334.

Chang, E. K. M., 1993: Downstream development of baroclinic waves as inferred from regression analysis. *J. Atmos. Sci.*, **50,** 2038–2053.

——, and I. Orlanski, 1993: On the dynamics of storm tracks. *J. Atmos. Sci.*, **50,** 999–1015.

——, and ——, 1994: On energy flux and group velocity of waves in baroclinic flows. *J. Atmos. Sci.*, **51,** 3823–3828.

Charney, J. G., 1947: The dynamics of long waves in a baroclinic westerly current. *J. Meteor.*, **4,** 135–163.

——, and M. E. Stern, 1962: On the stability of internal baroclinic jets in a rotating atmosphere. *J. Atmos. Sci.,* **19,** 159–172.

Davis, C. A., 1992a: Piecewise potential vorticity inversion. *J. Atmos. Sci.,* **49,** 1397–1411.

——, 1992b: A potential-vorticity diagnosis of the importance of initial structure and condensational heating in observed extratropical cyclogenesis. *Mon. Wea. Rev.,* **120,** 2409–2428.

——, 1993: Comments on "Decomposing the atmospheric flow using potential vorticity framework." *J. Atmos. Sci.,* **50,** 2065–2067.

——, and K. A. Emanuel, 1991: Potential vorticity diagnostics of cyclogenesis. *Mon. Wea. Rev.,* **119,** 1929–1953.

——, M. T. Stoelinga, and Y.-H. Kuo, 1993: The integrated effect of condensation in numerical simulations of extratropical cyclogenesis. *Mon. Wea. Rev.,* **121,** 2309–2330.

——, E. D. Grell, and M. A. Shapiro, 1996: The balanced dynamical nature of a rapidly intensifying oceanic cyclone. *Mon. Wea. Rev.,* **124,** 3–26.

Dey, C. H., 1989: The evolution of objective analysis methodology at the National Meteorological Center. *Wea. Forecasting,* **4,** 297–312.

Eady, E. T., 1949: Long waves and cyclone waves. *Tellus,* **1** (Part **3**), 33–52.

Farrell, B., 1985: Transient growth of damped baroclinic waves. *J. Atmos. Sci.,* **42,** 2718–2727.

——, 1989a: Optimal excitation of baroclinic waves. *J. Atmos. Sci.,* **46,** 1193–1206.

——, 1989b: Transient development in confluent and diffluent flow. *J. Atmos. Sci.,* **46,** 3279–3288.

Grotjahn, R., and J. Tribbia, 1995: On the mechanism of cyclogenesis as deduced from vertical axis tilts. *Tellus,* **47A,** 629–637.

Hakim, G. J., D. Keyser, and L. F. Bosart, 1996: The Ohio Valley wave-merger cyclogenesis event of 25–26 January 1978. Part II: Diagnosis using quasigeostrophic potential vorticity inversion. *Mon. Wea. Rev.,* **124,** 2176–2205.

Holopainen, E., and J. Kaurola, 1991: Decomposing the atmospheric flow using potential vorticity framework. *J. Atmos. Sci.,* **48,** 2614–2625.

——, and ——, 1993: Reply. *J. Atmos. Sci.,* **50,** 2068–2069.

Holton, J. R., 1993: *An Introduction to Dynamic Meteorology.* 3d ed. Academic Press, 511 pp.

Hoskins, B. J., 1990: Theory of extratropical cyclones. *Extratropical Cyclones: The Erik Palmén Memorial Volume,* C. Newton and E. Holopainen, Eds., Amer. Meteor. Soc., 63–80.

——, M. E. McIntyre, and A. W. Robertson, 1985: On the use and significance of isentropic potential vorticity maps. *Quart. J. Roy. Meteor. Soc.,* **111,** 877–946.

Kanamitsu, M., 1989: Description of the NMC global data assimilation and forecast system. *Wea. Forecasting,* **4,** 335–342.

Lefevre, R. J., 1995: Using the quasigeostrophic potential vorticity height tendency equation to diagnose the development of midtropospheric mobile troughs. Ph.D. thesis, Texas A&M University, 220 pp.

——, and J. W. Nielsen-Gammon, 1995: An objective climatology of mobile troughs in the Northern Hemisphere. *Tellus,* **47A,** 638–655.

Morgan, M. C., 1994: An observationally and dynamically determined basic state for the study of synoptic scale waves. Ph.D. thesis, Massachusetts Institute of Technology, 123 pp.

Nielsen-Gammon, J. W., 1995: Dynamical conceptual models of upper-level mobile trough formation: Comparison and application. *Tellus,* **47A,** 705–721.

Orlanski, I., and E. K. M. Chang, 1993: Ageostrophic geopotential fluxes in downstream and upstream development of baroclinic waves. *J. Atmos. Sci.,* **50,** 212–225.

——, and J. Katzfey, 1991: The life cycle of a cyclone wave in the Southern Hemisphere. Part I: Eddy energy budget. *J. Atmos. Sci.,* **48,** 1972–1998.

——, and J. Sheldon, 1993: A case of downstream baroclinic development over western North America. *Mon. Wea. Rev.,* **121,** 2929–2950.

——, and ——, 1995: Stages in the energetics of baroclinic systems. *Tellus,* **47A,** 605–628.

Palmén, E., and C. Newton, 1948: A study of the mean wind and temperature distribution in the vicinity of the polar front in winter. *J. Meteor.,* **5,** 220–226.

Parker, D. J., and A. J. Thorpe, 1995: The role of snow sublimation in frontogenesis. *Quart. J. Roy. Meteor. Soc.,* **121,** 763–782.

Petterssen, S., 1956: *Weather Analysis and Forecasting.* Vol. 1. 2d ed. McGraw-Hill, 428 pp.

Press, W. H., S. A. Teukolsky, W. T. Vetterling, and B. P. Flannery, 1992: *Numerical Recipes in FORTRAN: The Art of Scientific Computing.* 2d ed. Cambridge University Press, 963 pp.

Reed, R. J., M. T. Stoelinga, and Y.-H. Kuo, 1992: A model-aided study of the origin and evolution of the anomalously high potential vorticity in the inner region of a rapidly deepening marine cyclone. *Mon. Wea. Rev.,* **120,** 893–913.

Rivest, C., and B. F. Farrell, 1992: Upper-tropospheric synoptic-scale waves. Part II: Maintenance and excitation of quasi modes. *J. Atmos. Sci.,* **49,** 2120–2138.

——, C. A. Davis, and B. F. Farrell, 1992: Upper-tropospheric synoptic-scale waves. Part I: Maintenance as Eady normal modes. *J. Atmos. Sci.,* **49,** 2108–2119.

Rotunno, R., and M. Fantini, 1989: Petterssen's "Type B" cyclogenesis in terms of discrete, neutral Eady modes. *J. Atmos. Sci.,* **46,** 3599–3604.

Sanders, F., 1986: Explosive cyclogenesis in the west-central North Atlantic Ocean, 1981–84. Part I: Composite structure and mean behavior. *Mon. Wea. Rev.,* **114,** 1781–1794.

——, 1988: Life histories of mobile troughs in the upper westerlies. *Mon. Wea. Rev.,* **116,** 2629–2648.

Simmons, A. J., and B. J. Hoskins, 1979: The downstream and upstream development of unstable baroclinic waves. *J. Atmos. Sci.,* **36,** 1239–1254.

Snyder, C. M., and R. S. Lindzen, 1988: Upper-level baroclinic instability. *J. Atmos. Sci.,* **45,** 2445–2459.

——, and ——, 1991: Quasi-geostrophic wave-CISK in an unbounded baroclinic shear. *J. Atmos. Sci.,* **48,** 76–86.

Washington, W. M., and C. L. Parkinson, 1986: *An Introduction to Three-Dimensional Climate Modeling.* University Science Books, 422 pp.

Whitaker, J. S., and A. Barcilon, 1992: Genesis of mobile troughs in the upper westerlies. *J. Atmos. Sci.,* **49,** 2097–2107.

——, and C. A. Davis, 1994: Cyclogenesis in a saturated environment. *J. Atmos. Sci.,* **51,** 889–907.